arXiv:0905.3953v1 [cond-mat.mes-hall] 25 May 2009

Resonant Spectrum Analysis of the Conductance of Open Quantum System and Three Types of the Fano Parameter

Keita Sasada and Naomichi Hatano*
Department of Physics and Institute of Industrial Science,
University of Tokyo, Komaba, Meguro, Tokyo 153-8505, Japan

Gonzalo Ordonez†
Department of Physics, Butler University, 4600 Sunset Ave., Indianapolis, IN 46208, USA.

(Dated: May 25, 2009)

The main purpose of the present paper is to analyze the conductance of an N-site quantum dot with multiple semi-infinite leads. First, we obtain a simple conductance formula that contains only the local density of discrete eigenstates and the local density of states of the leads, where the discrete eigenstates consist of the bound states, the anti-bound states, the resonant states and the anti-resonant states. In other words, the conductance is given by the sum of all the simple poles in the complex energy plane. To our knowledge, this is the first time the effect of resonances on the conductance is shown exactly. Second, by using the above conductance formula, we show that the asymmetry of the Fano conductance peak arises from three origins, namely, from the interference between a resonant state and an anti-resonant state, between a resonant state and a bound state, and between two different states. Finally, we microscopically derive three types of the Fano parameter from the local density of discrete eigenstates, whereas in previous studies in the literature, the Fano parameter mainly has been used phenomenologically to describe the shape of an asymmetric conductance peak.

PACS numbers: 72.10.Bg; 73.21.La; 73.22.Dj; 73.23.Ad

I. INTRODUCTION

The electron conduction in nano-scale systems has been studied extensively in recent years [1, 2, 3, 4, 5, 6, 7, 8, 9, 10, 11, 12, 13, 14, 15, 16, 17, 18, 19]. The resonant transport is one of its interesting phenomena, where resonant states affect the conductance in its ballistic transport regime. Resonance is an intrinsic feature of open systems [17, 18, 20, 21, 22, 23, 24, 25, 26, 27, 28, 29, 30, 31, 32, 33, 34, 35, 36, 37, 38, 39, 40, 41, 42, 43, 44, 45, 46, 47, 48, 49, 50, 51, 52, 53, 54, 55, 56, 57, 58, 59, 60, 61, 62, 63, 64, 65, 66, 67, 68, 69, 70, 71, 72, 73, 74, 75, 76, 77, 78, 79, 80, 81]. When we use nano-devices, we inevitably attach leads to them. Hence the devices are always open systems and have resonant states; an electron comes into the device through a lead, is trapped in the confining potential of the device for a while with a finite lifetime, and may come out through another lead. This resonant conduction of mesoscopic systems has been intensely studied experimentally [9, 10, 11, 12, 13, 14, 15, 16, 19]; for example, the Fano resonance has attracted much attention. The theory of these open systems, however, has not been developed so much as applicable to the computation of the conductance of nano-scale systems.

We here consider a class of open quantum-dot systems, where all semi-infinite leads are attached to one site of a general N-site quantum dot. For this particular model, we rigorously transform the Landauer formula into a simple conductance formula expressed in terms of the discrete eigenstates, that is, the bound states, the resonant states, the anti-resonant states and the anti-bound states. To our knowledge, this is the first time the effect of resonances on the conductance is shown exactly.

Based on the simple conductance formula, we next discuss the symmetry of resonance peaks in the conductance. We are particularly interested in an asymmetric conductance peak, namely the Fano effect [82]. In the simplest theory of resonance scattering, a peak observed in, say, the scattering cross section would have a symmetric Breit-Wigner shape of a Lorentzian. In fact, some of the peaks are asymmetric. Fano proposed a theory explaining the asymmetric shape [82]. The asymmetric resonance peak has been thereby referred to as the Fano resonance. In 2002, K. Kobayashi *et al.* observed Fano resonance peaks in the conductance through an Aharonov-Bohm system with a quantum dot [9, 10] as well as through a T-shaped quantum dot [11, 12]. Asymmetric Fano peaks were clearly observed in the conductance.

It is a conventional understanding that the Fano effect arises from the coupling of continuous states in the leads and discrete states in the device [9, 10, 11, 12]. In contrast, we here stress the importance of the interference between resonant states [17] as well as between a resonant state and a bound state when we consider the Fano conductance peak. We show that the complex eigenvalues of the resonant states of the whole system, the quantum dot with the leads, form the asymmetric conductance peak.

The present paper is organized as follows. In Sec. II,

---

*Electronic address: hatano@iis.u-tokyo.ac.jp
†Electronic address: gordonez@butler.edu

we review the theory of resonant states in open quantum systems. In Sec. III, we express, for an N-site open quantum-dot model, the retarded and advanced Green's functions in terms of the discrete eigenstates. We thereby derive a conductance formula consisting only of the local density of discrete eigenstates and the local density of states of the leads. In Sec. IV, we show that the asymmetry of the Fano conductance peak arises from the interference between the resonant states as well as between a resonant state and a bound state.

II. RESONANT STATES

As a preparation for the main part of the present paper, we review in this section mathematics of the resonant state as an eigenfunction of the Schrödinger equation [18]. It is rather common to define a resonant state as a pole of the S matrix. In fact, there are two ways of defining the resonant state. The definition based on the S matrix may be called the indirect method [83]. We here use the direct method of its definition; that is, we describe it as an explicit eigenfunction of the Schrödinger equation [18, 20, 21, 22, 23, 24, 25, 26, 27, 28, 29, 30, 31, 32, 84].

Suppose that we have a scatterer with several semi-infinite leads attached to it. For simplicity and concreteness, we hereafter restrict ourselves to the tight-binding model for the lead Hamiltonians. The total Hamiltonian is of the form

$$H = H_{\mathrm{d}} + \sum_{\alpha} \left(H_\alpha + H_{d,\alpha} \right), \tag{1}$$

where H_{d} is the one-body Hamiltonian of the scatterer (namely, the dot Hamiltonian), H_α is the Hamiltonian of a lead α, and H_α is the coupling between the dot and the lead α. We assume that

$$H_\alpha = -t \sum_{x_\alpha=0}^{\infty} \left(|x_\alpha + 1\rangle\langle x_\alpha| + |x_\alpha\rangle\langle x_\alpha + 1| \right). \tag{2}$$

Therefore, the energy E_k and the wave number k of incoming and outgoing electrons are related through the dispersion relation

$$E_k \equiv -2t \cos k. \tag{3}$$

We can define the resonant state as a solution of the Schrödinger equation for the whole Hamiltonian H under the boundary conditions that the wave function has only out-going waves away from the scatterer [18, 20, 21, 22]. The condition is often called the Siegert condition [21]. More specifically, we seek discrete and generally complex eigenvalues E_n of the whole system H,

$$H|\psi_n\rangle = E_n|\psi_n\rangle, \tag{4}$$

$$\langle\tilde{\psi}_n|H = E_n\langle\tilde{\psi}_n|, \tag{5}$$

in the first Brillouin zone $-\pi < \mathrm{Re}\,k \leq \pi$ under the Siegert boundary condition as [18, 85, 86]

$$\langle x_\alpha|\psi_n\rangle = \langle\tilde{\psi}_n|x_\alpha\rangle \propto e^{ik_n|x_\alpha|} \tag{6}$$

for x_α on any lead α, where $|\psi_n\rangle$ is the right-eigenfunction and $\langle\tilde{\psi}_n|$ is the left-eigenfunction [24, 25, 26, 27, 28, 29, 30, 31, 32, 87, 88]. (Note that $\langle\tilde{\psi}_n|^\dagger \neq |\psi_n\rangle$

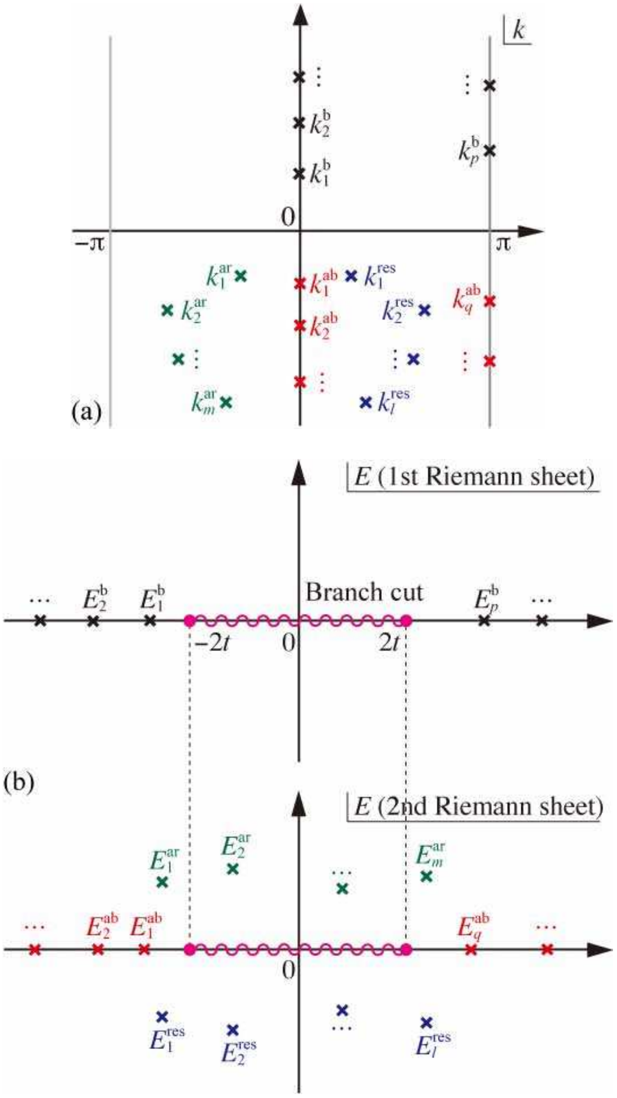

FIG. 1: (Color online) (a) Distribution of the eigen-wave-numbers k_p^{b} of the bound states (black crosses), k_l^{res} of the resonant states (blue crosses), k_m^{ar} of the anti-resonant states (green crosses), and k_q^{ab} of the anti-bound states (red crosses) on the complex wave-number plane. (b) Distribution of the eigenvalues E_p^{b} of the bound states (black crosses), E_l^{res} of the resonant states (blue crosses), E_m^{ar} of the anti-resonant states (green crosses), and E_q^{ab} of the anti-bound states (red crosses) on the complex energy plane. The upper and lower halves of the k plane respectively correspond to the first and second Riemann sheets of the E plane. A branch cut $-2t < E < 2t$ accompanied by two branch points $E = \pm 2t$ connect the two Riemann sheets.

in general.) The thus-obtained eigen-wave-number

$$k_n \equiv k_{\mathrm{r}n} + i\kappa_n \tag{7}$$

as well as the corresponding eigenenergy

$$E_n \equiv E_{\mathrm{r}n} + iE_{\mathrm{i}n} = -2t\cos k_n \tag{8}$$

are generally complex numbers. Note here that we have two Riemann sheets of E for the entire complex plane of k (Fig. 1). A branch cut $-2t < E < 2t$ with two branch points $E = \pm 2t$ connects the two Riemann sheets.

The discrete eigenstates thus obtained are classified as follows (Table I and Fig. 1). First, the eigenstates with $\kappa_n > 0$ are necessarily on the imaginary axis $\operatorname{Re} k = 0$ or on the edge of the Brillouin zone $\operatorname{Re} k = \pi$. (In systems with continuous space, the bound states exist only on the imaginary k axis; the bound states on the line $\operatorname{Re} k = \pi$ appear because the leads of the present system are lattice systems.) By putting $\kappa_n > 0$ in Eq. (6), we see that the eigenstates are in fact bound states. Hereafter, we use the subscript p and the superscript 'b' for the bound states as in k_p^{b} and E_p^{b}. The bound states with ${k_{\mathrm{r}}}_p^{\mathrm{b}} = 0$ have real negative eigenenergies $E_p^{\mathrm{b}} < -2t$ while the bound states with ${k_{\mathrm{r}}}_p^{\mathrm{b}} = \pi$ have real positive ones $E_p^{\mathrm{b}} > 2t$.

Next, the eigenstates in the fourth quadrant of the k plane are referred to as the resonant states. Hereafter, we use the subscript l and the superscript 'res' for the resonant states as in k_l^{res} and E_l^{res}. The corresponding eigenenergies are in the lower half of the second Riemann sheet of the E plane: ${E_{\mathrm{i}}}_l^{\mathrm{res}} < 0$.

Third, the eigenstates in the third quadrant of the k plane are referred to as the anti-resonant states. (In the context of the condensed-matter physics, some refer to a resonance in the form of a dip of the conductance as an anti-resonance. In the present terminology, this is just another resonance, different from the anti-resonant state here.) Hereafter, we use the subscript m and the superscript 'ar' for the resonant states as in k_m^{ar} and E_m^{ar}. The corresponding eigenenergies are in the upper half of the second Riemann sheet of the E plane: ${E_{\mathrm{i}}}_m^{\mathrm{ar}} > 0$. A resonant state and an anti-resonant state always appear in pair. The states of a pair are related to each other as

$$\begin{aligned}
|\psi_m^{\mathrm{ar}}\rangle &= \langle\tilde{\psi}_l^{\mathrm{res}}|^\dagger, \quad \text{and} \quad \langle\tilde{\psi}_m^{\mathrm{ar}}| = |\psi_l^{\mathrm{res}}\rangle^\dagger, && (9)\\
k_m^{\mathrm{ar}} &= -\left(k_l^{\mathrm{res}}\right)^*, \quad \text{or} &&\\
{k_{\mathrm{r}}}_m^{\mathrm{ar}} &= -{k_{\mathrm{r}}}_l^{\mathrm{res}} \quad \text{and} \quad \kappa_m^{\mathrm{ar}} = \kappa_l^{\mathrm{res}}, && (10)\\
E_m^{\mathrm{ar}} &= \left(E_l^{\mathrm{res}}\right)^*, \quad \text{or} &&\\
{E_{\mathrm{r}}}_m^{\mathrm{ar}} &= {E_{\mathrm{r}}}_l^{\mathrm{res}} \quad \text{and} \quad {E_{\mathrm{i}}}_m^{\mathrm{ar}} = -{E_{\mathrm{i}}}_l^{\mathrm{res}}. && (11)
\end{aligned}$$

We refer to a pair of the resonant state and the corresponding anti-resonant state as a resonant-state pair.

Some systems have additional states on the negative part of the imaginary k axis or on the negative part of the edge of the Brillouin zone $\operatorname{Re} k = \pi$. Such states often appear when resonant and anti-resonant states of a pair collide on the axes. We refer to them as anti-bound states [89] and use the subscript q and the superscript 'ab' as in k_q^{ab} and E_q^{ab}. Anti-bound states possess real eigenenergies but on the second Riemann sheet and still have properties of the resonant states such as diverging wave functions.

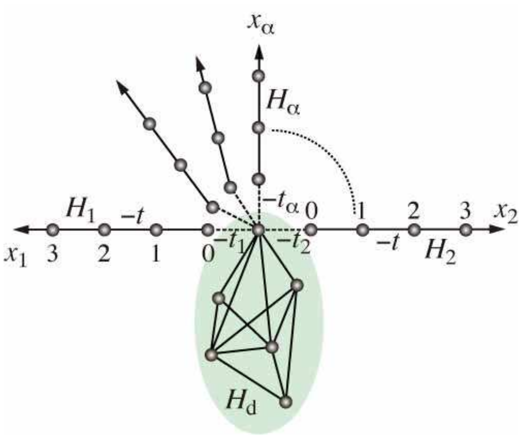

FIG. 2: The open quantum N-site dot with multiple leads that we consider in present paper.

III. RESONANT SPECTRUM ANALYSIS OF AN OPEN QUANTUM N-SITE DOT

In the present section, we discuss an N-site extension of the Friedrichs-Fano (Newns-Anderson) model [82, 88, 90, 91, 92, 93, 94, 95]. We derive a remarkably simple conductance formula for the model. The formula contains only the local density of discrete eigenstates and the local density of states of the leads.

We consider a one-body Hamiltonian of an N-site dot with semi-infinite leads $\{\alpha\}$ attached to it (Fig. 2);

$$H = H_{\mathrm{d}} + \sum_\alpha \left(H_\alpha + H_{\mathrm{d},\alpha}\right) \tag{12}$$

with

$$\begin{aligned}
H_{\mathrm{d}} \equiv & \sum_{i=0}^{N-1} \varepsilon_i |d_i\rangle\langle d_i| \\
& - \sum_{0\leqslant i<j\leqslant N-1} v_{ij}\left(|d_i\rangle\langle d_j| + |d_j\rangle\langle d_i|\right), && (13)\\
H_\alpha \equiv & -t\sum_{x_\alpha=0}^{\infty}\left(|x_\alpha+1\rangle\langle x_\alpha| + |x_\alpha\rangle\langle x_\alpha+1|\right), && (14)\\
H_{\mathrm{d},\alpha} \equiv & -t_\alpha\left(|x_\alpha=0\rangle\langle d_0| + |d_0\rangle\langle x_\alpha=0|\right), && (15)
\end{aligned}$$

where ε_i, v_{ij}, t and t_α are all real parameters with $v_{ij} = v_{ji}$. The Hamiltonian H_{d} is the tight-binding Hamiltonian of the N-site dot, while H_α is the tight-binding Hamiltonian of the one-dimensional semi-infinite lead α and $H_{\mathrm{d},\alpha}$ is the hopping between a site d_0 on the central dot and the end site $x_\alpha = 0$ of the lead α. We

TABLE I: Classification of the discrete eigenstates.

Bound states	${k_{\mathrm{r}}}_p^{\mathrm{b}} = 0$	$\kappa_p^{\mathrm{b}} > 0$	first Riemann sheet	$E_p^{\mathrm{b}} < -2t$
	${k_{\mathrm{r}}}_p^{\mathrm{b}} = \pi$	$\kappa_p^{\mathrm{b}} > 0$	first Riemann sheet	$E_p^{\mathrm{b}} > 2t$
Anti-bound states	${k_{\mathrm{r}}}_q^{\mathrm{ab}} = 0$	$\kappa_q^{\mathrm{ab}} < 0$	second Riemann sheet	$E_q^{\mathrm{ab}} < -2t$
	${k_{\mathrm{r}}}_q^{\mathrm{ab}} = \pi$	$\kappa_q^{\mathrm{ab}} < 0$	second Riemann sheet	$E_q^{\mathrm{ab}} > 2t$
Resonant states	${k_{\mathrm{r}}}_l^{\mathrm{res}} > 0$	$\kappa_l^{\mathrm{res}} < 0$	second Riemann sheet	${E_{\mathrm{i}}}_l^{\mathrm{res}} < 0$
Anti-resonant states	${k_{\mathrm{r}}}_m^{\mathrm{ar}} < 0$	$\kappa_m^{\mathrm{ar}} < 0$	second Riemann sheet	${E_{\mathrm{i}}}_l^{\mathrm{ar}} > 0$

attach all the leads to the single site d_0 of the dot; this is due to a technical requirement that appears below. The system is an N-site extension of the Friedrichs-Fano model [82, 88, 90, 91, 92, 93, 94, 95]. We will obtain the conductance $\mathcal{G}_{\alpha\to\beta}(E)$ from the lead α to the lead β in the form

$$\mathcal{G}_{\alpha\to\beta}(E) = \frac{G^{\max}_{\alpha\to\beta}}{2}\left[1 \pm \sqrt{1 - \left(\frac{\rho_{\mathrm{eigen}}(E)}{\rho_{\mathrm{leads}}(E)}\right)^2}\,\right], \tag{16}$$

where

$$\begin{cases} \rho_{\mathrm{eigen}}(E) & \equiv \dfrac{1}{2\pi}\displaystyle\sum_{n\in p,q,l,m} \dfrac{\langle d_0|\psi_n\rangle\langle\tilde{\psi}_n|d_0\rangle}{E-E_n}, \\ \rho_{\mathrm{leads}}(E) & \equiv \dfrac{1}{\sum_\alpha (t_\alpha/t)^2\,\pi\sqrt{4t^2-E^2}}. \end{cases} \tag{17}$$

Here $\rho_{\mathrm{eigen}}(E)$ is the local density of discrete eigenstates of the whole system on the site d_0 and $\rho_{\mathrm{leads}}(E)$ is the local density of states of the lead Hamiltonian $\sum_\alpha H_\alpha$. The subscripts p, q, l and m respectively denote sets of the bound states, the anti-bound states, the resonant states and the anti-resonant states.

Let us describe the derivation of Eq. (16) hereafter. We can obtain the exact expression of the scattering states of the system (12), namely the Friedrichs solution [90] $|\psi_k^{\mathrm{F}}\rangle$, with the eigenvalue $E_k = -2t\cos k$; see Appendix A. The completeness with respect to the scattering states is given by [96]

$$1 = \sum_p |\psi_p^{\mathrm{b}}\rangle\langle\tilde{\psi}_p^{\mathrm{b}}| + \int_{\mathrm{BZ}} \frac{dk}{2\pi} |\psi_k^{\mathrm{F}}\rangle\langle\tilde{\psi}_k^{\mathrm{F}}|, \tag{18}$$

where $|\psi_p^{\mathrm{b}}\rangle$ is a bound state and $|\psi_k^{\mathrm{F}}\rangle$ is a scattering state given in Appendix A, and we used the notation

$$|\psi_k^{\mathrm{F}}\rangle\langle\tilde{\psi}_k^{\mathrm{F}}| \equiv \sum_\alpha |\psi_{k,\alpha}^{\mathrm{F}}\rangle\langle\tilde{\psi}_{k,\alpha}^{\mathrm{F}}|. \tag{19}$$

We first express the retarded and advanced Green's functions in the spectral representation;

$$G^{\mathrm{R}}(E) = \sum_p \frac{|\psi_p^{\mathrm{b}}\rangle\langle\tilde{\psi}_p^{\mathrm{b}}|}{E-E_p^{\mathrm{b}}} + \int_{C_{\mathrm{BZ}}^{\mathrm{R}}} \frac{dk}{2\pi}\frac{|\psi_k^{\mathrm{F}}\rangle\langle\tilde{\psi}_k^{\mathrm{F}}|}{E-E_k}, \tag{20}$$

$$G^{\mathrm{A}}(E) = \sum_p \frac{|\psi_p^{\mathrm{b}}\rangle\langle\tilde{\psi}_p^{\mathrm{b}}|}{E-E_p^{\mathrm{b}}} + \int_{C_{\mathrm{BZ}}^{\mathrm{A}}} \frac{dk}{2\pi}\frac{|\psi_k^{\mathrm{F}}\rangle\langle\tilde{\psi}_k^{\mathrm{F}}|}{E-E_k}, \tag{21}$$

where the integration contours $C_{\mathrm{BZ}}^{\mathrm{R}}$ and $C_{\mathrm{BZ}}^{\mathrm{A}}$ cover the Brillouin zone as indicated in Fig. 3.

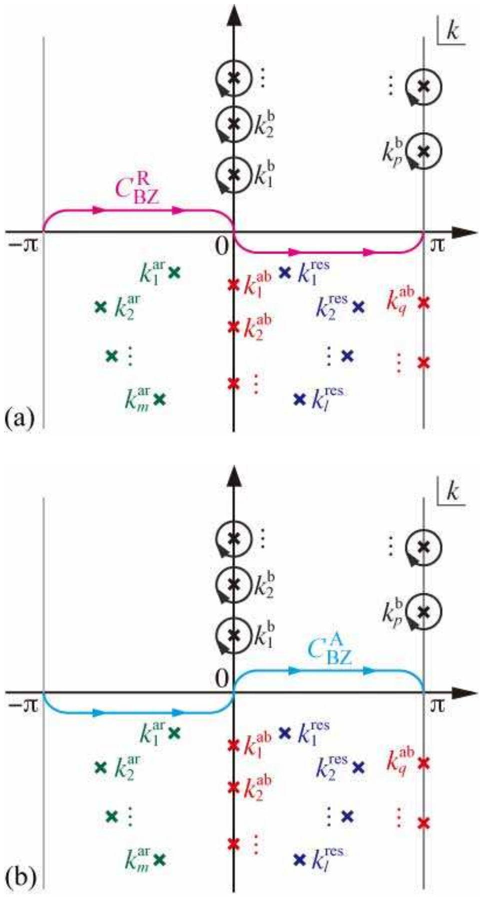

FIG. 3: (Color online) (a) The integration contour $C_{\mathrm{BZ}}^{\mathrm{R}}$ (purple curve) for the retarded Green's function $G^{\mathrm{R}}(E)$ and (b) the integration contour $C_{\mathrm{BZ}}^{\mathrm{A}}$ (cyan curve) for the advanced Green's function $G^{\mathrm{A}}(E)$, with the circular (gray) contours extracting bound states in the complex wave-number plane.

Next, we replace the integration contours $C_{\mathrm{BZ}}^{\mathrm{R}}$ and $C_{\mathrm{BZ}}^{\mathrm{A}}$ with the ones shown in Fig. 4. Then the retarded Green's function $G^{\mathrm{R}}(E)$ acquires the residual integrals of the resonant states k_l^{res}, which lie in the fourth quadrant, while the advanced Green's function $G^{\mathrm{A}}(E)$ acquires the residual integrals of the anti-resonant states k_m^{ar}, which lie in

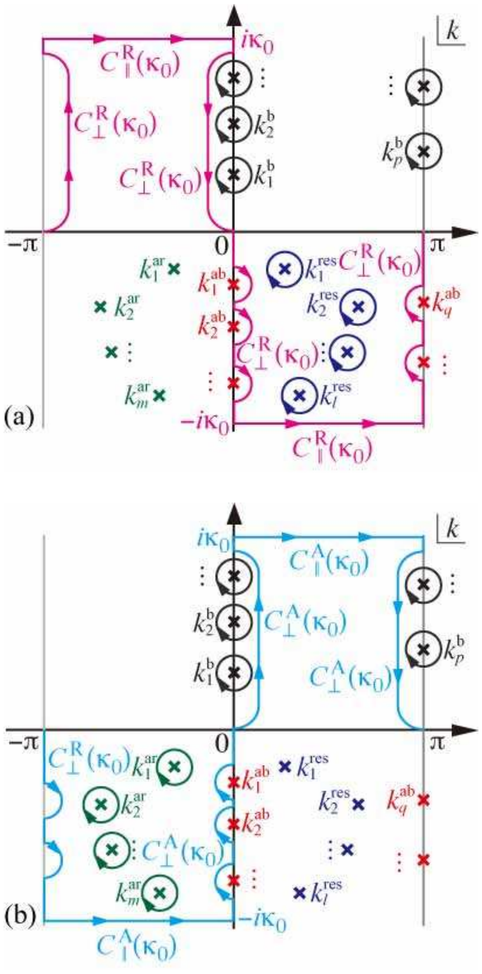

FIG. 4: (Color online) (a) The integration contours $C_\perp^{\mathrm{R}}(\kappa_0)$ and $C_\parallel^{\mathrm{R}}(\kappa_0)$ (purple curves) for the retarded Green's function $G^{\mathrm{R}}(E)$, modified for extracting the resonant states (blue crosses) in the complex wave-number plane. (b) The integration contours $C_\perp^{\mathrm{A}}(\kappa_0)$ and $C_\parallel^{\mathrm{A}}(\kappa_0)$ (cyan curves) for the advanced Green's function $G^{\mathrm{A}}(E)$, modified for extracting the anti-resonant states (green crosses).

the third quadrant:

$$\oint_{C(k=k_l^{\mathrm{res}})} \frac{dk}{2\pi} \frac{|\psi_k^{\mathrm{F}}\rangle\langle\tilde{\psi}_k^{\mathrm{F}}|}{E-E_k} = \frac{|\psi_l^{\mathrm{res}}\rangle\langle\tilde{\psi}_l^{\mathrm{res}}|}{E-E_l^{\mathrm{res}}}, \tag{22}$$

$$\oint_{C(k=k_m^{\mathrm{ar}})} \frac{dk}{2\pi} \frac{|\psi_k^{\mathrm{F}}\rangle\langle\tilde{\psi}_k^{\mathrm{F}}|}{E-E_k} = \frac{|\psi_m^{\mathrm{ar}}\rangle\langle\tilde{\psi}_m^{\mathrm{ar}}|}{E-E_m^{\mathrm{ar}}}. \tag{23}$$

We then have

$$G^{\mathrm{R}}(E) = \sum_p \frac{|\psi_p^{\mathrm{b}}\rangle\langle\tilde{\psi}_p^{\mathrm{b}}|}{E-E_p^{\mathrm{b}}} + \sum_l \frac{|\psi_l^{\mathrm{res}}\rangle\langle\tilde{\psi}_l^{\mathrm{res}}|}{E-E_l^{\mathrm{res}}} + \lim_{\kappa_0\to+\infty}\int_{C_\perp^{\mathrm{R}}(\kappa_0)+C_\parallel^{\mathrm{R}}(\kappa_0)} \frac{dk}{2\pi}\frac{|\psi_k^{\mathrm{F}}\rangle\langle\tilde{\psi}_k^{\mathrm{F}}|}{E-E_k}, \tag{24}$$

$$G^{\mathrm{A}}(E) = \sum_p \frac{|\psi_p^{\mathrm{b}}\rangle\langle\tilde{\psi}_p^{\mathrm{b}}|}{E-E_p^{\mathrm{b}}} + \sum_m \frac{|\psi_m^{\mathrm{ar}}\rangle\langle\tilde{\psi}_m^{\mathrm{ar}}|}{E-E_m^{\mathrm{ar}}} + \lim_{\kappa_0\to+\infty}\int_{C_\perp^{\mathrm{A}}(\kappa_0)+C_\parallel^{\mathrm{A}}(\kappa_0)} \frac{dk}{2\pi}\frac{|\psi_k^{\mathrm{F}}\rangle\langle\tilde{\psi}_k^{\mathrm{F}}|}{E-E_k}. \tag{25}$$

Here $C_\parallel^{\mathrm{R}}(\kappa_0)$ indicates the sum of the paths parallel to the real axis and $C_\perp^{\mathrm{R}}(\kappa_0)$ the sum of the paths perpendicular to the real axis including the contributions from the anti-bound states. Note that κ_0 of the modified integration contour must be positive and greater than the imaginary parts of all the resonant eigen-wave-numbers.

At this point, we sum up the retarded and advanced Green's functions;

$$\begin{aligned} &G^{\mathrm{R}}(E)+G^{\mathrm{A}}(E) \\ &= 2\sum_p \frac{|\psi_p^{\mathrm{b}}\rangle\langle\tilde{\psi}_p^{\mathrm{b}}|}{E-E_p^{\mathrm{b}}} + \sum_l \frac{|\psi_l^{\mathrm{res}}\rangle\langle\tilde{\psi}_l^{\mathrm{res}}|}{E-E_l^{\mathrm{res}}} + \sum_m \frac{|\psi_m^{\mathrm{ar}}\rangle\langle\tilde{\psi}_m^{\mathrm{ar}}|}{E-E_m^{\mathrm{ar}}} \\ &\quad + \lim_{\kappa_0\to\infty}\int_{C_\perp^{\mathrm{R}}(\kappa_0)+C_\perp^{\mathrm{A}}(\kappa_0)} \frac{dk}{2\pi}\frac{|\psi_k^{\mathrm{F}}\rangle\langle\tilde{\psi}_k^{\mathrm{F}}|}{E-E_k} \\ &\quad + \lim_{\kappa_0\to\infty}\int_{C_\parallel^{\mathrm{R}}(\kappa_0)+C_\parallel^{\mathrm{A}}(\kappa_0)} \frac{dk}{2\pi}\frac{|\psi_k^{\mathrm{F}}\rangle\langle\tilde{\psi}_k^{\mathrm{F}}|}{E-E_k}. \end{aligned} \tag{26}$$

The sum of the contributions of the integration contour $C_\perp^{\mathrm{R}}(\kappa_0)$ and $C_\perp^{\mathrm{A}}(\kappa_0)$ is equal to the contribution of the bound states and anti-bound states except for the sign;

$$\begin{aligned} &\lim_{\kappa_0\to\infty}\int_{C_\perp^{\mathrm{R}}(\kappa_0)+C_\perp^{\mathrm{A}}(\kappa_0)} \frac{dk}{2\pi}\frac{|\psi_k^{\mathrm{F}}\rangle\langle\tilde{\psi}_k^{\mathrm{F}}|}{E-E_k} \\ &\qquad = -\sum_p \frac{|\psi_p^{\mathrm{b}}\rangle\langle\tilde{\psi}_p^{\mathrm{b}}|}{E-E_p^{\mathrm{b}}} + \sum_q \frac{|\psi_q^{\mathrm{ab}}\rangle\langle\tilde{\psi}_q^{\mathrm{ab}}|}{E-E_q^{\mathrm{ab}}}. \end{aligned} \tag{27}$$

On the other hand, we proved that the contributions of the parallel integration contours $C_\parallel^{\mathrm{R}}(\kappa_0)$ and $C_\parallel^{\mathrm{A}}(\kappa_0)$ vanish for the states on the central dot; i.e. for $|d_i\rangle$ and $|d_j\rangle$ with any i and j, we have

$$\lim_{\kappa_0\to+\infty}\int_{C_\parallel^{\mathrm{R}}(\kappa_0)+C_\parallel^{\mathrm{A}}(\kappa_0)} \frac{dk}{2\pi}\frac{\langle d_i|\psi_k^{\mathrm{F}}\rangle\langle\tilde{\psi}_k^{\mathrm{F}}|d_j\rangle}{E-E_k} = 0. \tag{28}$$

See Appendix B for the proof. Equation (28) does not seem to hold if the semi-infinite leads are not attached to a single site of the central dot. This is why we focused on the present system (12).

Thus we find that the sum of the retarded and advanced Green's functions is equal to the contributions of

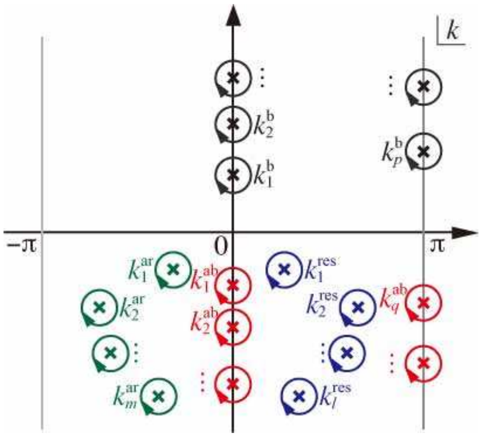

FIG. 5: (Color online) Summation of the modified integration contours for the retarded and advanced Green's functions in the complex wave-number plane results in the sum of the contributions of all discrete eigenstates containing the bound states (black crosses), the resonant states (blue crosses), the anti-resonant states (green crosses) and the anti-bound states (red crosses).

only the discrete eigenstates for the states on the central dot, $\{|d_i\rangle\}$, (Fig. 5);

$$\langle d_i| \left(G^{\mathrm{A}}(E)+G^{\mathrm{R}}(E)\right)|d_j\rangle = \langle d_i|\Lambda(E)|d_j\rangle, \tag{29}$$

where

$$\Lambda(E) \equiv \sum_{n\in p,q,l,m} \frac{|\psi_n\rangle\langle\tilde{\psi}_n|}{E-E_n}. \tag{30}$$

We also use the fact that the difference between the retarded and advanced Green's functions is generally given by [2]

$$G^{\mathrm{A}}(E)-G^{\mathrm{R}}(E) = iG^{\mathrm{R}}(E)\Gamma(E)G^{\mathrm{A}}(E), \tag{31}$$

where

$$\begin{aligned}\Gamma(E) &\equiv i\left(V_{\mathrm{eff}}^{\mathrm{R}}(E)-V_{\mathrm{eff}}^{\mathrm{A}}(E)\right)|d_0\rangle\langle d_0| \\ &= \sum_\alpha \Gamma^{(\alpha)}(E)\end{aligned} \tag{32}$$

with the self-energies of the semi-infinite leads

$$V_{\mathrm{eff}}^{\mathrm{R}}(E) \equiv \sum_\alpha \left(\frac{t_\alpha}{t}\right)^2 \frac{E-i\sqrt{4t^2-E^2}}{2}, \tag{33}$$

$$V_{\mathrm{eff}}^{\mathrm{A}}(E) \equiv \sum_\alpha \left(\frac{t_\alpha}{t}\right)^2 \frac{E+i\sqrt{4t^2-E^2}}{2}, \tag{34}$$

and

$$\Gamma^{(\alpha)}(E) \equiv \left(\frac{t_\alpha}{t}\right)^2 \sqrt{4t^2-E^2}|d_0\rangle\langle d_0|; \tag{35}$$

see Appendix C for derivations of the self-energies. (The relation (31) holds for arbitrary sites, not restricted to the states of the central dot, $\{|d_i\rangle\}$.) Equation (29) shows that the real part of the Green's function is given by the discrete eigenstates, while Eq. (31) shows that the imaginary part of the Green's function is given by the inverse of the van Hove singularities at the branch points $E=\pm 2t$ [2].

The simultaneous matrix equations (29) and (31) results in the matrix Riccati equations

$$\begin{aligned}&\langle d_i|\left\{G^{\mathrm{R}}(E)\left(i\Gamma(E)\right)G^{\mathrm{R}}(E)\right. \\ &\qquad \left. +G^{\mathrm{R}}(E)\left[2+\left(i\Gamma(E)\right)\Lambda(E)\right]+\Lambda(E)\right\}|d_j\rangle = 0,\end{aligned} \tag{36}$$

$$\begin{aligned}&\langle d_i|\left\{G^{\mathrm{A}}(E)\left(-i\Gamma(E)\right)G^{\mathrm{A}}(E)\right. \\ &\qquad \left. -\left[2+\Lambda(E)\left(-i\Gamma(E)\right)\right]G^{\mathrm{A}}(E)+\Lambda(E)\right\}|d_j\rangle = 0.\end{aligned} \tag{37}$$

The solution gives each Green's function in terms of the contribution of the discrete eigenstates, $\Lambda(E)$, and the contribution of the branch-point singularities, $\Gamma(E)$. Using the fact that $\langle d_0|\Gamma|d_0\rangle$ is the only non-zero element of the matrix $\langle d_i|\Gamma|d_j\rangle$ for the present system (12, we first solve the above equations for $i=j=0$, then for $i=0$ with general j and for $j=0$ with general i, and finally for general i and j. Denoting $\langle d_i|G^{\mathrm{R/A}}(E)|d_j\rangle = G_{ij}^{\mathrm{R/A}}(E)$, $\langle d_i|\Lambda(E)|d_j\rangle = \Lambda_{ij}(E)$ and $\langle d_i|\Gamma(E)|d_j\rangle = \Gamma_{ij}(E)$, we obtain the final solution as

$$G_{ij}^{\mathrm{R}}(E) = \frac{\Lambda_{ij}(E)}{2} + \frac{\Lambda_{i0}(E)\Lambda_{0j}(E)}{\Lambda_{00}(E)}\frac{1\pm\sqrt{1-\Omega(E)^2}}{2i\Omega}, \tag{38}$$

$$G_{ij}^{\mathrm{A}}(E) = \frac{\Lambda_{ij}(E)}{2} - \frac{\Lambda_{i0}(E)\Lambda_{0j}(E)}{\Lambda_{00}(E)}\frac{1\pm\sqrt{1-\Omega(E)^2}}{2i\Omega}, \tag{39}$$

where

$$\Omega(E) \equiv \frac{1}{2}\Gamma_{00}(E)\Lambda_{00}(E). \tag{40}$$

The sign in front of the square root of Eqs. (38) and (39) is chosen according to the rule given in Appendix D.

Using the Fisher-Lee relation [97], we arrive at the conductance $\mathcal{G}_{\alpha\to\beta}(E)$ from the lead α to the lead β in the form

$$\begin{aligned}\mathcal{G}_{\alpha\to\beta}(E) &\equiv \frac{2e^2}{h}\mathrm{Tr}\left(\Gamma^{(\beta)}(E)G^{\mathrm{R}}(E)\Gamma^{(\alpha)}(E)G^{\mathrm{A}}(E)\right) \\ &= \frac{2e^2}{h}\Gamma_{00}^{(\beta)}(E)G_{00}^{\mathrm{R}}(E)\Gamma_{00}^{(\alpha)}(E)G_{00}^{\mathrm{A}}(E) \\ &= \frac{G_{\alpha\to\beta}^{\max}}{2}\left[1\pm\sqrt{1-\Omega(E)^2}\right],\end{aligned} \tag{41}$$

where

$$G_{\alpha\to\beta}^{\max} \equiv \frac{2e^2}{h}\left(\frac{2t_\alpha t_\beta}{\sum_\gamma t_\gamma^2}\right)^2 \tag{42}$$

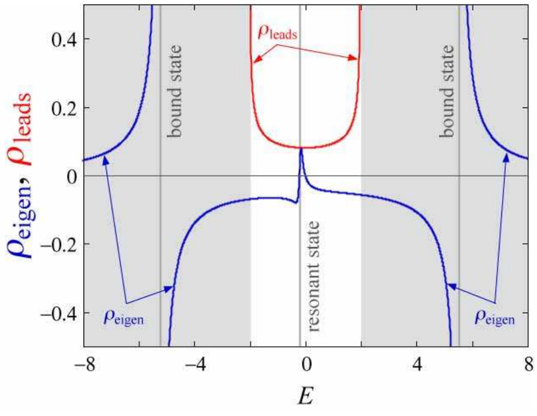

FIG. 6: (Color online) The local density of the discrete eigenstates, $\rho_{\rm eigen}(E)$ (blue curves), and the local density of the lead states, $\rho_{\rm leads}(E)$ (red curve). The plots are for a two-site dot with two leads. The parameter values are $t_1/t = t_2/t = 1$, $\varepsilon_0/t = 5$, $\varepsilon_1/t = 0$ and $v_{01}/t = v_{10}/t = 1$. The gray vertical lines indicate the two bound states ($E_1^{\rm b} = -5.20735\ldots$, $E_2^{\rm b} = 5.55278\ldots$), as well as the real part of the resonant-state pair ($E^{\rm res/ar} = -0.172712\ldots \mp i0.0689508\ldots$). The structure of $\rho_{\rm eigen}(E)$ around the resonant-state pair is continuous for real E. The shaded areas indicate the outside of the energy band, $|E| > 2t$.

is the maximum possible conductance from the lead α to the lead β. (In the transformation of Eq. (41), we again used the fact that the matrix $\Gamma^{(\alpha)}$ has only the $(0,0)$ element for the present system (12); see Eq. (32).) Equation (41) gives a remarkably simple formula

$$\mathcal{G}_{\alpha\to\beta}(E) = \frac{G^{\max}_{\alpha\to\beta}}{2}\left[1 \pm \sqrt{1-\left(\frac{\rho_{\rm eigen}(E)}{\rho_{\rm leads}(E)}\right)^2}\,\right], \qquad (43)$$

where

$$\begin{cases} \rho_{\rm eigen}(E) & \equiv \dfrac{\Lambda_{00}(E)}{2\pi} = \dfrac{1}{2\pi}\displaystyle\sum_{n\in p,q,l,m}\frac{\langle d_0|\psi_n\rangle\langle\tilde{\psi}_n|d_0\rangle}{E-E_n} \\ \rho_{\rm leads}(E) & \equiv \dfrac{1}{\pi\Gamma_{00}(E)} = \dfrac{1}{\sum_\alpha (t_\alpha/t)^2\,\pi\sqrt{4t^2-E^2}}. \end{cases} \qquad (44)$$

Here $\rho_{\rm eigen}(E)$ is the local density of discrete eigenstates of the whole system H on the site d_0, whereas $\rho_{\rm leads}(E)$ is the local density of states of the lead Hamiltonians $\sum_\alpha H_\alpha$, which has the van Hove singularities at the band edges $E = \pm 2t$. Note that $\rho_{\rm eigen}(E)$ has singularities at the discrete eigenvalues, whereas $\rho_{\rm leads}(E)$ has singularities at the branch points. The conductance itself has singularities due to the discrete eigenstates but not due to branch points. We exemplify $\rho_{\rm eigen}(E)$ and $\rho_{\rm leads}(E)$ in Fig. 6 for a two-site dot with two leads with $t_1/t = t_2/t = 1$, $\varepsilon_0/t = 5$, $\varepsilon_1/t = 0.5$ and $v_{01}/t = v_{10}/t = 0.5$.

To summarize the present section, we reveal the effect of resonances on the conductance explicitly and rigorously. To our knowledge, this is for the first time the conductance is exactly given in terms of the sum of simple poles of the discrete eigenstates.

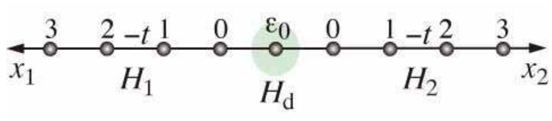

FIG. 7: A point contact d_0 with two leads.

IV. QUANTUM INTERFERENCE EFFECT OF DISCRETE EIGENSTATES

In the present section, we argue that the Fano conductance arises as a result of interference between discrete eigenstates. The conductance formula (43) has a square of the local density of discrete eigenstates. Therefore, we have crossing terms within a resonant-state pair (between a resonant state and an anti-resonant state), between two resonant-state pairs (two sets of a resonant state and an anti-resonant state), and between a resonant-state pair and a bound state. We show in the present section that discrete eigenvalues decide the symmetry or the asymmetry of the conductance peaks in addition to the location of the conductance peaks, using several examples. We thereby derive the Fano parameter microscopically. In Subsecs. A, B, and C of the present section, we consider the system (12) with the following restrictions: only two leads $\alpha = 1,2$; the coupling $t_1 = t_2 = t$; the number of sites in the dot $N = 1,2,3$. We consider the effect of changing t_α in Sec. IV D. Throughout the present section, we computed the conductance using the Fisher-Lee relation (41) and obtained all discrete eigenvalues solving Eq. (C30).

A. Point contact system: $N = 1$

First we show the conductance as well as the discrete eigenvalues of the one-site dot with two leads, namely the point contact shown in Fig. 7. There are only two bound states and no resonant state. We plot in Fig. 8 the conductance with the eigenvalues of the two bound states for $\varepsilon_0/t = 0, 1, 1.5, 2, 2.5$. The conductance of the point contact has no peculiar behavior such as the Breit-Wigner peak or the Fano peak. Upon increasing the potential ε_0, the eigenvalues of the two bound states move away from the branch points $E = \pm 2t$. This decreases the contribution of the local density of the discrete eigenstates $\rho_{\rm eigen}(E)$ and hence deflates the conductance gradually.

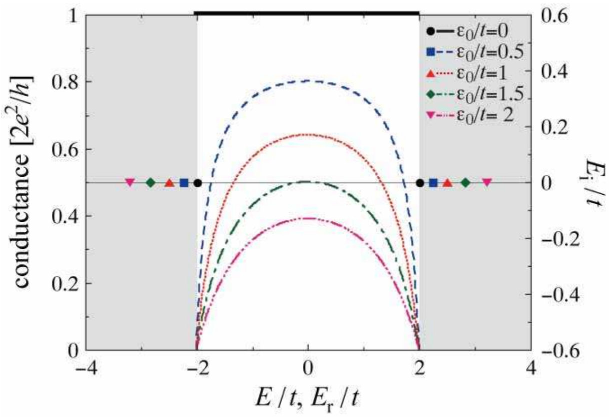

FIG. 8: The energy dependence of the conductance (the left axis) and the discrete eigenvalues of the bound states (the right axis) for the one-site dot with $\varepsilon_0/t = 0$, 1, 1.5, 2, 2.5.

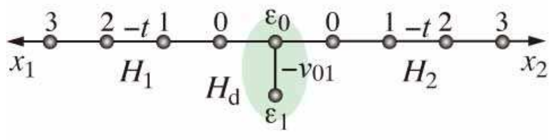

FIG. 9: A two-site quantum dot with two leads.

B. T-shaped quantum-dot system: $N = 2$

We next show the conductance and the discrete eigenvalues of the two-site quantum dot with two leads, namely a T-shaped quantum dot shown in Fig. 9. This system is a minimal model that possesses a resonant-state pair (a resonant state and the corresponding anti-resonant state) and may be directly related to Fano's original argument [82]. We plot in Fig. 10 the conductance, the eigenvalues of the two bound states, E_1^{b} and E_2^{b}, and the eigenvalues of the resonant-state pair, E^{res} and E^{ar}, for $\varepsilon_0/t = 0$, 1, 3, 5, $\varepsilon_1 = 0$ and $v_{01}/t = v_{10}/t = 1$.

We have a Breit-Wigner dip for $\varepsilon_0 = 0$, but for $\varepsilon_0 \neq 0$, we have an asymmetric peak, namely the Fano conductance peak. Maruyama *et al.* [98] claimed that the asymmetry of the conductance peak of the T-shaped quantum dot is proportional to ε_0. We here discuss the asymmetry from the viewpoint of interference among the discrete eigenstates.

The conductance formula (43) contains the square of the sum over the discrete eigenvalues of the form

$$\Omega(E)^2 \equiv \left(\frac{\rho_{\mathrm{eigen}}(E)}{\rho_{\mathrm{leads}}(E)}\right)^2 = \frac{\left(\rho^{\mathrm{b}}(E) + \rho^{\mathrm{pair}}(E)\right)^2}{\left(\rho_{\mathrm{leads}}(E)\right)^2}, \quad (45)$$

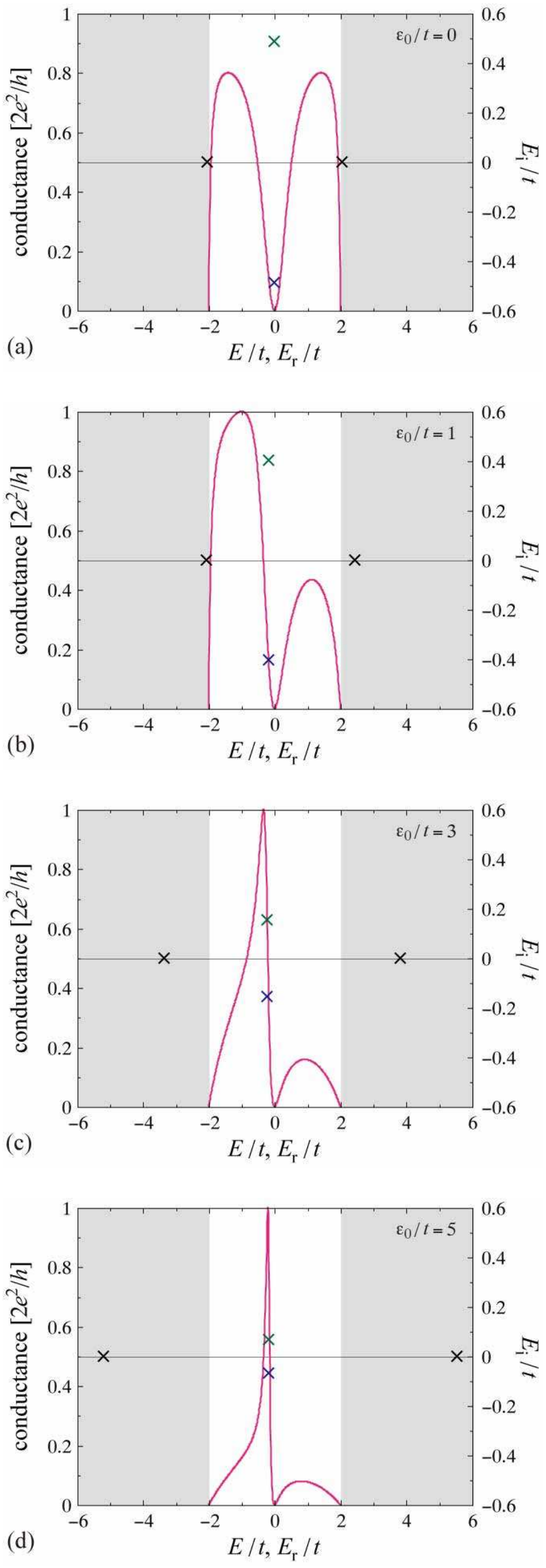

FIG. 10: (a) The ε_0 dependence of the conductance (the left axis) and the discrete eigenvalues (the right axis) for the two-site dot with (a) $\varepsilon_0/t = 0$, (b) $\varepsilon_0/t = 1$, (c) $\varepsilon_0/t = 3$ and (d) $\varepsilon_0/t = 5$. Here we fixed $\varepsilon_1/t = 0$ and $v_{01}/t = v_{10}/t = 1$.

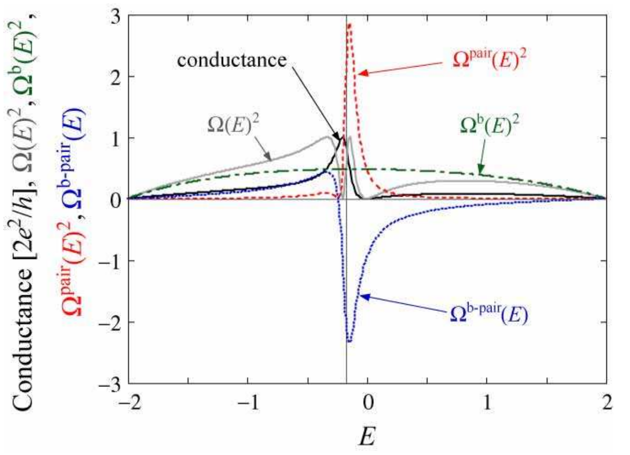

FIG. 11: (Color online) The quantities $\Omega(E)^2$ (gray curve), $\Omega^{\mathrm{b}}(E)^2$ (chained green curve), $\Omega^{\mathrm{pair}}(E)^2$ (broken red curve) and $\Omega^{\text{b-pair}}(E)$ (dotted blue curve), defined in Eqs. (45)–(51), plotted with the conductance (solid black curve), Eq. (41), or Eq. (43). The system is the two-site quantum dot. We fixed $\varepsilon_0/t = 5$, $\varepsilon_1/t = 0$ and $v_{01}/t = v_{10}/t = 1$. The gray vertical line indicates the real part of the resonant eigenvalue $E_{\mathrm{r}}^{\mathrm{res}} = -0.172712\ldots$.

where

$$\rho^{\mathrm{b}}(E) \equiv \sum_{p=1,2} \frac{1}{2\pi} \frac{\langle d_0|\psi_p^{\mathrm{b}}\rangle\langle\tilde{\psi}_p^{\mathrm{b}}|d_0\rangle}{E - E_p^{\mathrm{b}}}, \tag{46}$$

$$\rho^{\mathrm{pair}}(E) \equiv \frac{1}{2\pi}\frac{\langle d_0|\psi^{\mathrm{res}}\rangle\langle\tilde{\psi}^{\mathrm{res}}|d_0\rangle}{E - E^{\mathrm{res}}} + \frac{1}{2\pi}\frac{\langle d_0|\psi^{\mathrm{ar}}\rangle\langle\tilde{\psi}^{\mathrm{ar}}|d_0\rangle}{E - E^{\mathrm{ar}}}. \tag{47}$$

Since the conductance formula (43) is given in the form

$$G \propto \frac{\Omega(E)^2}{1 \mp \sqrt{1 - \Omega(E)^2}}, \tag{48}$$

the symmetry or the asymmetry of the quantity $\Omega(E)^2$ is directly reflected on the symmetry or the asymmetry of the conductance peak. Equation (45) therefore implies that the symmetry or the asymmetry of the conductance peak is strongly affected by crossing terms, or the interference between states with discrete eigenvalues. We hereafter show that the Fano conductance peak arises from two types of the interference, or two types of crossing terms. First, we have a crossing term within the resonant-state pair, or the interference between the resonant state and the anti-resonant state. Second, we have a crossing term between the bound states and the resonant-state pair.

We compare in Fig. 11 the following quantities:

$$\Omega^{\mathrm{b}}(E)^2 \equiv \frac{\left(\rho^{\mathrm{b}}(E)\right)^2}{\left(\rho_{\mathrm{leads}}(E)\right)^2}, \tag{49}$$

$$\Omega^{\mathrm{pair}}(E)^2 \equiv \frac{\left(\rho^{\mathrm{pair}}(E)\right)^2}{\left(\rho_{\mathrm{leads}}(E)\right)^2}, \tag{50}$$

$$\Omega^{\text{b-pair}}(E) \equiv \frac{2\rho^{\mathrm{b}}(E)\rho^{\mathrm{pair}}(E)}{\left(\rho_{\mathrm{leads}}(E)\right)^2}, \tag{51}$$

The second quantity (50) contains a crossing term between the resonant state and the anti-resonant state. The third quantity (51) contains crossing terms between the resonant state and a bound state as well as crossing terms between the anti-resonant state and a bound state. We can see in Fig. 11 that the asymmetry of the conductance peak comes partly from the asymmetry of the term $\Omega^{\mathrm{pair}}(E)$ and partly from the crossing term $\Omega^{\text{b-pair}}(E)$. The quantity $\Omega^{\mathrm{b}}(E)$ is almost symmetric.

In order to derive the Fano parameters for the asymmetry of the two terms $\Omega^{\mathrm{pair}}(E)$ and $\Omega^{\text{b-pair}}(E)$ microscopically, we expand the terms (50) and (51) in the neighborhood of $E = E_{\mathrm{r}}^{\mathrm{res}} = E_{\mathrm{r}}^{\mathrm{ar}}$ by using the normalized energy

$$\tilde{E} \equiv \frac{E - E_{\mathrm{r}}^{\mathrm{res}}}{|E_{\mathrm{i}}^{\mathrm{res}}|}. \tag{52}$$

We first rewrite $\rho^{\mathrm{pair}}(E)$ in the forms

$$\rho^{\mathrm{pair}}(E) = \frac{\tilde{N}e^{i\theta}/2}{E - (E_{\mathrm{r}}^{\mathrm{res}} + iE_{\mathrm{i}}^{\mathrm{res}})} + \text{c.c.}, \tag{53}$$

where we express the coefficient of the local density of the resonant state with the amplitude $\tilde{N}$ and the phase θ:

$$\tilde{N}e^{i\theta} \equiv \frac{\langle d_0|\psi^{\mathrm{res}}\rangle\langle\tilde{\psi}^{\mathrm{res}}|d_0\rangle}{\pi}. \tag{54}$$

Note that this is generally a complex number because the left-eigenvector $\langle\tilde{\psi}^{\mathrm{res}}|$ is not generally Hermitian conjugate to the right-eigenvector $|\psi^{\mathrm{res}}\rangle$ for a resonant state (see Eq. (9)). We then rewrite the local density of the resonant-state pair in the form

$$\begin{aligned}\rho^{\mathrm{pair}}(E) &= \tilde{N}\frac{(E - E_{\mathrm{r}}^{\mathrm{res}})\cos\theta + |E_{\mathrm{i}}^{\mathrm{res}}|\sin\theta}{(E - E_{\mathrm{r}}^{\mathrm{res}})^2 + |E_{\mathrm{i}}^{\mathrm{res}}|^2} \\ &= \frac{\tilde{N}}{|E_{\mathrm{i}}^{\mathrm{res}}|}\frac{\sin\theta + \tilde{E}\cos\theta}{1 + \tilde{E}^2},\end{aligned} \tag{55}$$

or

$$\Omega^{\mathrm{pair}}(E)^2 \propto \left(\frac{q^{\mathrm{pair}} + \tilde{E}}{1 + \tilde{E}^2}\right)^2, \tag{56}$$

where

$$q^{\mathrm{pair}} \equiv \tan\theta. \tag{57}$$

The parameter (57) controls the asymmetry of the term (50) and hence may be called the Fano parameter, although Eq. (56) is different from the form originally derived by Fano [82]:

$$G \sim \frac{\left(q+\tilde{E}\right)^2}{1+\tilde{E}^2}. \tag{58}$$

The asymmetry caused by the above interference between a resonant state and the corresponding anti-resonant state may be missing from Fano's argument.

On the other hand, the crossing term (51) produces asymmetry of Fano's original form (58). In order so see this, we approximate the local density of two bound states as

$$\rho^{\mathrm{b}}(E) \simeq \rho^{\mathrm{b}}(E_{\mathrm{r}}^{\mathrm{res}}) + \rho^{\mathrm{b}'}(E_{\mathrm{r}}^{\mathrm{res}})\left|E_{\mathrm{i}}^{\mathrm{res}}\right|\tilde{E} \tag{59}$$

in the neighborhood of $E = E_{\mathrm{r}}^{\mathrm{res}}$. We therefore have the crossing term between the resonant-state pair and the two bound states as

$$\Omega^{\text{b-pair}}(E) \equiv \frac{2\rho^{\mathrm{pair}}(E)\rho^{\mathrm{b}}(E)}{\left(\rho_{\mathrm{leads}}(E)\right)^2} \sim \frac{r+s\tilde{E}+t\tilde{E}^2}{1+\tilde{E}^2}, \tag{60}$$

where

$$r \equiv \frac{\rho^{\mathrm{b}}(E_{\mathrm{r}}^{\mathrm{res}})}{\left|E_{\mathrm{i}}^{\mathrm{res}}\right|}\sin\theta, \tag{61}$$

$$s \equiv \frac{\rho^{\mathrm{b}}(E_{\mathrm{r}}^{\mathrm{res}})}{\left|E_{\mathrm{i}}^{\mathrm{res}}\right|}\cos\theta + \rho^{\mathrm{b}'}(E_{\mathrm{r}}^{\mathrm{res}})\sin\theta, \tag{62}$$

$$t \equiv \rho^{\mathrm{b}'}(E_{\mathrm{r}}^{\mathrm{res}})\cos\theta. \tag{63}$$

In order to derive a Fano parameter $q^{\text{b-pair}}$ that controls the asymmetry of the term $\Omega^{\text{b-pair}}(E)$, we extract the form on the right-hand side of Eq. (58) by putting

$$\frac{r+s\tilde{E}+t\tilde{E}^2}{1+\tilde{E}^2} = a + b\frac{\left(q^{\text{b-pair}}+\tilde{E}\right)^2}{1+\tilde{E}^2}, \tag{64}$$

We obtain the Fano parameter $q^{\text{b-pair}}$ by solving the equation

$$s\left(q^{\text{b-pair}}\right)^2 - 2(r-t)q^{\text{b-pair}} - s = 0 \tag{65}$$

and choose the solution with the same sign as s. This controls the asymmetry of the term (51), a Fano parameter that is different from the one given by Eq. (57), but that conforms to Fano's original form (58).

We show in Fig. 12 how the two Fano parameters q^{pair} and $q^{\text{b-pair}}$ depend on the system parameter ε_0. In the particular case of Fig. 12, $q^{\text{b-pair}}$ tends to dominate over q^{pair} as we increase the system parameter ε_0. This is in coordination with the decrease of $|E_{\mathrm{i}}^{\mathrm{res}}|$. We can see in Eq. (62) that a small imaginary part $|E_{\mathrm{i}}^{\mathrm{res}}|$ causes a particularly strong asymmetry of the term $\Omega^{\text{b-pair}}(E)$. This is indeed demonstrated in Fig. 10, where, as we increase ε_0, the asymmetry rapidly develops while the the resonant eigenvalue approaches the real axis. Incidentally, the present system has the particle-hole symmetry $E \leftrightarrow -E$ for $\varepsilon_0 = \varepsilon_1 = 0$, and hence $q^{\mathrm{pair}} = q^{\text{b-pair}} = 0$, for which the resonance peak takes the form of a symmetric Lorentzian as shown in Fig. 10(a).

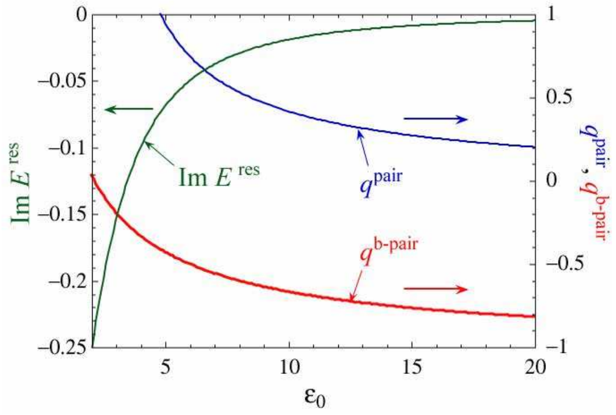

FIG. 12: (Color online) The Fano parameters q^{pair} (blue curve) and $q^{\text{b-pair}}$ (red curve) for the two-site dot, plotted with the imaginary part of the resonant eigenvalue $E_{\mathrm{i}}^{\mathrm{res}}$. Use the right axis for the Fano parameters and the left axis for the resonant eigenvalue. (Note that the horizontal axis does not start from $\varepsilon_0 = 0$. We omitted the part $0 \leq \varepsilon_0 < 2$ to avoid confusion because the structure of the spectrum is drastically different in that region.) We fixed $\varepsilon_1/t = 0$ and $v_{01}/t = v_{10}/t = 1$.

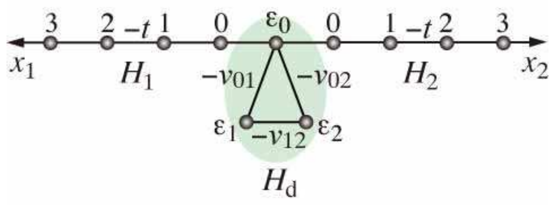

FIG. 13: The three-site quantum dot with two leads.

C. Three-site quantum-dot system: $N = 3$

Third, we discuss the conductance of the three-site quantum dot with two leads shown in Fig. 13. This system have two resonant states for some parameter values. This situation was not considered in Fano's argument [82]. We show in Fig. 14 the conductance, the eigenvalues of the two bound states, E_1^{b} and E_2^{b}, as well as the eigenvalues of the two resonant-state pairs, E_1^{res}, E_1^{ar}, E_2^{res} and E_2^{ar}, for $\varepsilon_1/t = -1.5, -1, -0.5, 0$ with $\varepsilon_0/t = 0$, $\varepsilon_2/t = 0.5$, $v_{01}/t = v_{10}/t = 0.8$, $v_{02}/t = v_{20}/t = 0.5$ and $v_{12}/t = v_{21}/t = 0.4$. Upon increasing the parameter ε_1, the conductance dip that is generated by the resonant state on the left-hand side, E_1^{res}, approaches to the other conductance dip that is generated by the resonant state on the right-hand side, E_2^{res}. Then the latter conductance peak develops strong asymmetry.

For the present system, we have yet another Fano parameter due to a crossing term between one resonant-state pair and the other resonant-state pair. The conductance formula (43) contains the square of the sum

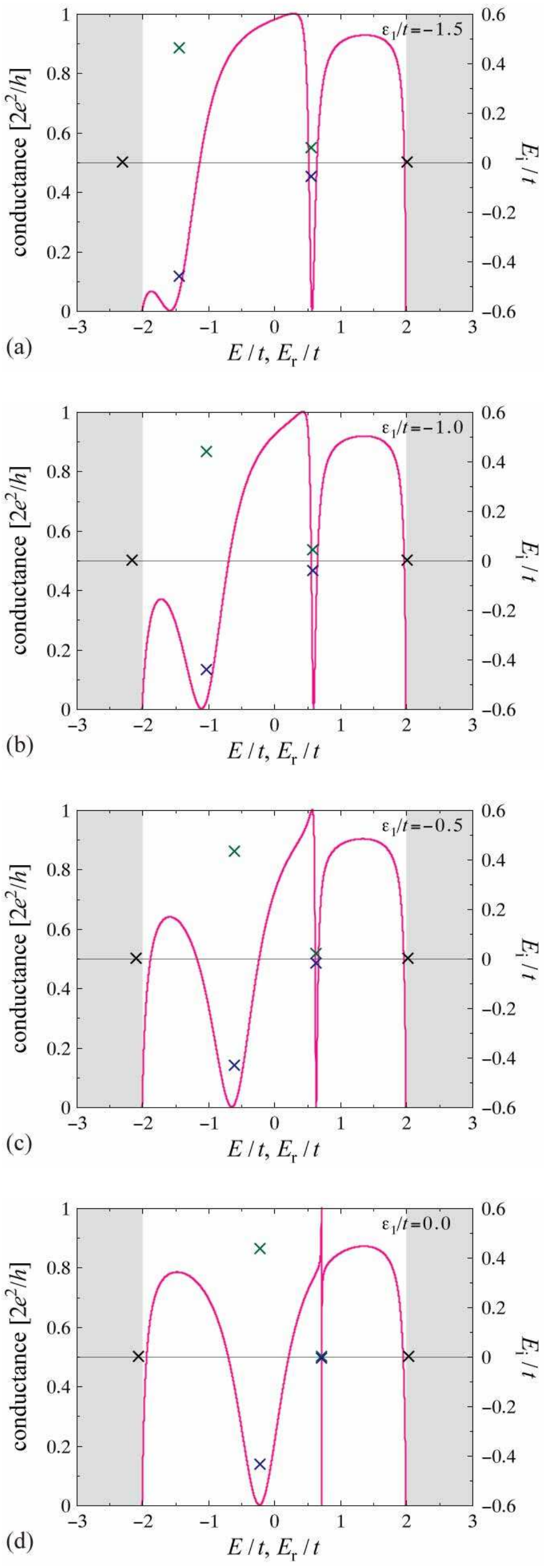

FIG. 14: The conductance (curve for the left axis) for the three-site dot with (a) $\varepsilon_1/t = -1.5$, (b) $\varepsilon_1/t = -1.0$, (c) $\varepsilon_1/t = -0.5$ and (d) $\varepsilon_1/t = 0$, plotted with all the discrete eigenvalues (crosses for the right axis). We fixed $\varepsilon_0/t = 0$, $\varepsilon_2/t = 0.5$, $v_{01}/t = v_{10}/t = 0.8$, $v_{02}/t = v_{20}/t = 0.5$ and $v_{12}/t = v_{21}/t = 0.4$.

over the discrete eigenvalues of the form

$$\Omega(E)^2 = \frac{\left(\rho^{\mathrm{b}}(E) + \rho_1^{\mathrm{pair}}(E) + \rho_2^{\mathrm{pair}}(E)\right)^2}{\left(\rho_{\mathrm{leads}}(E)\right)^2}, \tag{66}$$

where

$$\rho^{\mathrm{b}}(E) \equiv \sum_{p=1,2} \frac{1}{2\pi} \frac{\langle d_0|\psi_p^{\mathrm{b}}\rangle\langle\tilde{\psi}_p^{\mathrm{b}}|d_0\rangle}{E - E_p^{\mathrm{b}}}, \tag{67}$$

$$\rho_l^{\mathrm{pair}}(E) \equiv \frac{1}{2\pi} \frac{\langle d_0|\psi_l^{\mathrm{res}}\rangle\langle\tilde{\psi}_l^{\mathrm{res}}|d_0\rangle}{E - E_l^{\mathrm{res}}} + \frac{1}{2\pi} \frac{\langle d_0|\psi_l^{\mathrm{ar}}\rangle\langle\tilde{\psi}_l^{\mathrm{ar}}|d_0\rangle}{E - E_l^{\mathrm{ar}}} \quad \text{for } l = 1, 2. \tag{68}$$

We compare in Fig. 15 the following quantities:

$$\Omega^{\mathrm{b}}(E)^2 \equiv \frac{\left(\rho^{\mathrm{b}}(E)\right)^2}{\left(\rho_{\mathrm{leads}}(E)\right)^2}, \tag{69}$$

$$\Omega_l^{\mathrm{pair}}(E)^2 \equiv \frac{\left(\rho_l^{\mathrm{pair}}(E)\right)^2}{\left(\rho_{\mathrm{leads}}(E)\right)^2} \quad \text{for } l = 1, 2, \tag{70}$$

$$\Omega_l^{\text{b-pair}}(E) \equiv \frac{2\rho^{\mathrm{b}}(E)\rho_l^{\mathrm{pair}}(E)}{\left(\rho_{\mathrm{leads}}(E)\right)^2} \quad \text{for } l = 1, 2, \tag{71}$$

$$\Omega^{\text{pair-pair}}(E) \equiv \frac{2\rho_1^{\mathrm{pair}}(E)\rho_2^{\mathrm{pair}}(E)}{\left(\rho_{\mathrm{leads}}(E)\right)^2}, \tag{72}$$

We can see that the following three terms are asymmetric: first, $\Omega_2^{\mathrm{pair}}(E)^2$, which contains the crossing term between the resonant eigenstate ψ_2^{res} and the anti-resonant eigenstate ψ_2^{ar}; second, $\Omega_2^{\text{b-pair}}(E)$, which is the crossing term between the bound states $(\psi_1^{\mathrm{b}}, \psi_2^{\mathrm{b}})$ and the resonant-state pair $(\psi_2^{\mathrm{res}}, \psi_2^{\mathrm{ar}})$; third, $\Omega^{\text{pair-pair}}(E)$, which is the crossing term between the two resonant-state pairs $(\psi_1^{\mathrm{res}}, \psi_1^{\mathrm{ar}})$ and $(\psi_2^{\mathrm{res}}, \psi_2^{\mathrm{ar}})$.

In order to derive the Fano parameters for the asymmetry of the three terms, we expand the terms (70)–(72) in the neighborhood of $E = E_{\mathrm{r2}}^{\mathrm{res}}$ by using the normalized energy

$$\tilde{E} \equiv \frac{E - E_{\mathrm{r2}}^{\mathrm{res}}}{|E_{\mathrm{i2}}^{\mathrm{res}}|}. \tag{73}$$

We can analyze the terms $\Omega_2^{\mathrm{pair}}(E)$ and $\Omega_2^{\text{b-pair}}(E)$ in the same way as in the previous subsection. We again use the expression

$$\tilde{N}e^{i\theta} \equiv \frac{\langle d_0|\psi_2^{\mathrm{res}}\rangle\langle\tilde{\psi}_2^{\mathrm{res}}|d_0\rangle}{\pi}. \tag{74}$$

Then the Fano parameter controlling the asymmetry of the term $\Omega_2^{\mathrm{pair}}(E)$ is given by

$$q_2^{\mathrm{pair}} = \tan\theta. \tag{75}$$

Following the same logic as in Eqs. (52)–(65), we obtain the Fano parameter that controls the asymmetry of the term $\Omega_2^{\text{b-pair}}(E)$ by solving

$$s\left(q_2^{\text{b-pair}}\right)^2 - 2(r-t)q_2^{\text{b-pair}} - s = 0, \tag{76}$$

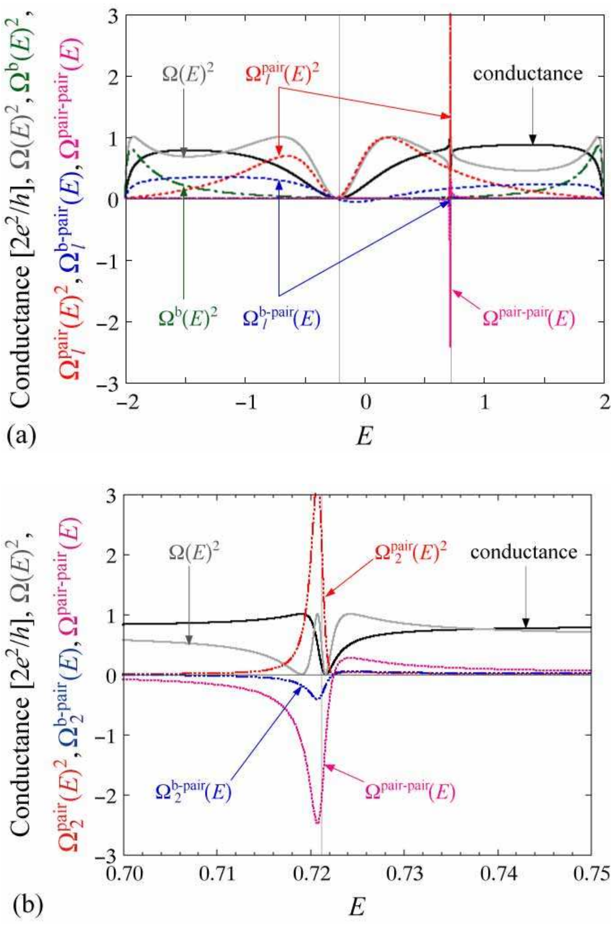

FIG. 15: (Color online) The quantities $\Omega(E)^2$ (gray curve), $\Omega^{\rm b}(E)^2$ (green curve), $\Omega_l^{\rm pair}(E)^2$ (broken and chained red curves), $\Omega_l^{\rm b\text{-}pair}(E)$ (broken and chained blue curves) and $\Omega^{\rm pair\text{-}pair}(E)$ (dotted purple curve), defined in Eq. (66)–(72), plotted with the conductance (solid curve), Eq. (41), or Eq. (43). The vertical gray lines indicate the real parts of the resonant eigenvalues $E = E^{\rm res}_{\rm r1} = -0.211544\ldots$ and $E = E^{\rm res}_{\rm r2} = 0.721170\ldots$. (b) shows the part of (a) around $E = E^{\rm res}_{\rm r2}$ with the plots of the conductance (solid curve), $\Omega(E)^2$ (gray curve), $\Omega_2^{\rm pair}(E)^2$ (chained red curve), $\Omega_2^{\rm b\text{-}pair}(E)$ (chained blue curve) and $\Omega^{\rm pair\text{-}pair}(E)$ (dotted purple curve). The system is the three-site dot. We fixed $\varepsilon_0/t = 0$, $\varepsilon_1/t = 0$, $\varepsilon_2/t = 0.5$, $v_{01}/t = v_{10}/t = 0.8$, $v_{02}/t = v_{20}/t = 0.5$ and $v_{12}/t = v_{21}/t = 0.4$.

where

$$r \equiv \frac{\rho^{\rm b}(E^{\rm res}_{\rm r2})}{|E^{\rm res}_{\rm i2}|}\sin\theta, \tag{77}$$

$$s \equiv \frac{\rho^{\rm b}(E^{\rm res}_{\rm r2})}{|E^{\rm res}_{\rm i2}|}\cos\theta + \rho^{\rm b\prime}(E^{\rm res}_{\rm r2})\sin\theta, \tag{78}$$

$$t \equiv \rho^{\rm b\prime}(E^{\rm res}_{\rm r2})\cos\theta. \tag{79}$$

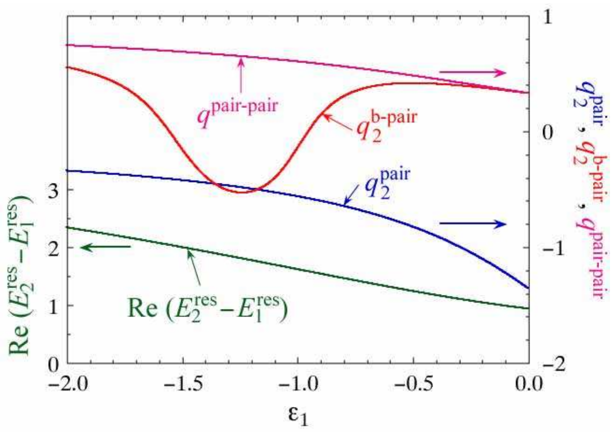

FIG. 16: (Color online) The Fano parameters $q_2^{\rm pair}$ (blue curve), $q_2^{\rm b\text{-}pair}$ (red curve) and $q^{\rm pair\text{-}pair}$ (purple curve), plotted with the difference of the real parts of the two resonant eigenvalues, $E^{\rm res}_{\rm r2} - E^{\rm res}_{\rm r1}$. Use the right axis for the Fano parameters and the left axis for the eigenvalue difference. We fixed $\varepsilon_0/t = 0$, $\varepsilon_2/t = 0.5$, $v_{01}/t = v_{10}/t = 0.8$, $v_{02}/t = v_{20}/t = 0.5$ and $v_{12}/t = v_{21}/t = 0.4$.

Next, in order to discuss the quantity $\Omega^{\rm pair\text{-}pair}(E)$, we use the expansion

$$\rho_1^{\rm pair}(E) \simeq \rho_1^{\rm pair}(E^{\rm res}_{\rm r2}) + \rho_1^{\rm pair\prime}(E^{\rm res}_{\rm r2})\,|E^{\rm res}_{\rm i2}|\,\tilde{E}. \tag{80}$$

We then approximately have the crossing term between the two resonant-state pairs as

$$\Omega^{\rm pair\text{-}pair}(E) \equiv \frac{2\rho_1^{\rm pair}(E)\rho_2^{\rm pair}(E)}{\left(\rho_{\rm leads}(E)\right)^2} \sim \frac{r' + s'\tilde{E} + t'\tilde{E}^2}{1+\tilde{E}^2} \tag{81}$$

with

$$r' \equiv \frac{\rho_1^{\rm pair}(E^{\rm res}_{\rm r2})}{|E^{\rm res}_{\rm i2}|}\sin\theta, \tag{82}$$

$$s' \equiv \frac{\rho_1^{\rm pair}(E^{\rm res}_{\rm r2})}{|E^{\rm res}_{\rm i2}|}\cos\theta + \rho_1^{\rm pair\prime}(E^{\rm res}_{\rm r2})\sin\theta, \tag{83}$$

$$t' \equiv \rho_1^{\rm pair\prime}(E^{\rm res}_{\rm r2})\cos\theta, \tag{84}$$

We thus have yet another Fano parameter $q^{\rm pair\text{-}pair}$ as the solution of

$$s'\left(q^{\rm pair\text{-}pair}\right)^2 - 2(r'-t')q^{\rm pair\text{-}pair} - s' = 0. \tag{85}$$

We show in Fig. 16 how the three Fano parameters $q_2^{\rm pair}$, $q_2^{\rm b\text{-}pair}$ and $q^{\rm pair\text{-}pair}$ depend on the system parameter ε_1. In the particular case of Fig. 16, the third Fano parameter $q^{\rm pair\text{-}pair}$ is the greatest in most of the range. This may be due to the following reason. The first term of s' for the parameter $q^{\rm pair\text{-}pair}$ contains the Lorentzian

$$\rho_1^{\rm pair}(E^{\rm res}_{\rm r2}) \sim \left[(E^{\rm res}_{\rm r1} - E^{\rm res}_{\rm r2})^2 + E^{\rm res\,2}_{\rm i1}\right]^{-1}. \tag{86}$$

Therefore, s' grows fast as the resonant-state pair $E^{\rm res}_{\rm r1}$ approaches the resonant-state pair $E^{\rm res}_{\rm r2}$ up until $|E^{\rm res}_{\rm r1} - E^{\rm res}_{\rm r2}| \sim |E^{\rm res}_{\rm i1}|$. This is in contrast to the first term of s for the parameter $q_2^{\text{b-pair}}$, which contains

$$\rho^{\rm b}(E^{\rm res}_{\rm r2}) \sim \left(E^{\rm b}_p - E^{\rm res}_{\rm r2}\right)^{-1} \tag{87}$$

for $p = 1, 2$. This is indeed demonstrated in Fig. 14, where, as we increase ε_1, the asymmetry rapidly develops while the resonant-state pair $(E^{\rm res}_1, E^{\rm ar}_1)$ approaches $(E^{\rm res}_2, E^{\rm ar}_2)$.

D. The effect of the hopping energy t_α between the central dot and the leads

Finally, we briefly show the effect of the hopping energy t_α between the central dot and the lead α. We here use the case of the three-site dot with two leads with $t_1 = t_2 \neq t$, $\varepsilon_0/t = 0$, $\varepsilon_1/t = 0$, $\varepsilon_2/t = 0.5$, $v_{01}/t = v_{10}/t = 0.8$, $v_{02}/t = v_{20}/t = 0.5$ and $v_{12}/t = v_{21}/t = 0.4$. For $t_1 = t_2 < t/\sqrt{2}$, there are three resonant-state pairs and no bound states. We have corresponding three sharp peaks in the weakly coupled case $t_1/t = t_2/t = 0.1$ as in Fig. 17 (a). Upon increasing the hopping energy $t_1 = t_2$, the second peak corresponding to the resonant-state pair with the least modulus of the imaginary part develops asymmetry. At $t_1/t = t_2/t = 1/\sqrt{2}$, the resonant and anti-resonant states of a resonant-state pair collide and become two anti-bound states, which leaves two resonant-state pairs. For $t_1/t = t_2/t > 1/\sqrt{2}$, the second peak continuously develop the asymmetry. (The anti-bound states become bound states before $t_1 = t_2 = t$.)

V. CONCLUSION

We carried out the spectrum analysis of the open quantum N-site dot with multiple leads. We obtained the simple conductance formula (43) in terms of the local density of discrete eigenstates (the bound states, the resonant states, the anti-resonant states and the anti-bound states), $\rho_{\rm eigen}(E)$, and the local density of states of the leads, $\rho_{\rm leads}(E)$. To our knowledge, this is the first time the conductance is exactly give by the sum of all the simple poles.

We then showed that the Fano conductance arises from the crossing terms of three origins; first between a pair of a resonant state and an anti-resonant state, second between a resonant-state pair and a bound state, and finally between two resonant-state pairs. We also presented microscopic derivation of the Fano parameter.

The analysis in the present paper is applicable only to non-interacting systems. It is an interesting and challenging problem to generalize the present approach to interacting systems. The Kondo effect, for example, has been observed in recent experiments on quantum dots

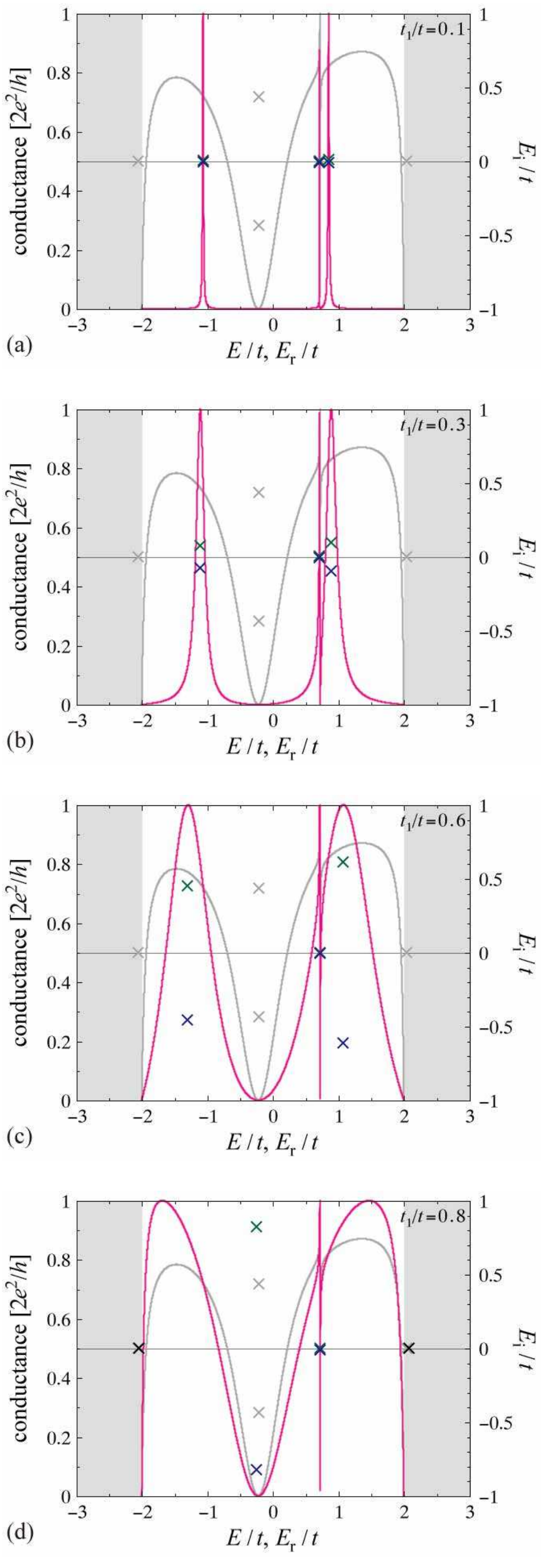

FIG. 17: The conductance (curve for the left axis) for the three-site dot with (a) $t_1/t = t_2/t = 0.1$, (b) $t_1/t = t_2/t = 0.3$, (c) $t_1/t = t_2/t = 0.6$ and (d) $t_1/t = t_2/t = 0.8$, plotted with all the discrete eigenvalues (crosses for the right axis) The gray curves and the gray crosses indicate the conductance and the discrete eigenvalues for $t_1/t = t_2/t = 1$, the same data as plotted in Fig. 14 . We fixed $\varepsilon_0/t = 0$, $\varepsilon_1/t = 0$, $\varepsilon_2/t = 0.5$, $v_{01}/t = v_{10}/t = 0.8$, $v_{02}/t = v_{20}/t = 0.5$ and $v_{12}/t = v_{21}/t = 0.4$.

and attracts much theoretical interest. The present approach may be particularly useful in analyzing the interplay between the Fano resonance and Kondo resonance.

Acknowledgments

This work is supported by Grant-in-Aid for Scientific Research No. 17340115 from the Ministry of Education, Culture, Sports, Science and Technology as well as by Core Research for Evolutional Science and Technology (CREST) of Japan Science and Technology Agency.

APPENDIX A: FRIEDRICHS SOLUTION OF THE SYSTEM (12)

In the present appendix, we solve the Lippmann-Schwinger equation for the present system (12) to obtain the Friedrichs solution [90] of the scattering states. The Lippmann-Schwinger equation may be written down as

$$\left|\psi^{\mathrm{F}}_{k,\alpha}\right\rangle = |k,\alpha\rangle + \frac{1}{E_k - H_0 + i\delta} H_1 \left|\psi^{\mathrm{F}}_{k,\alpha}\right\rangle, \tag{A1}$$

where

$$\begin{aligned} H_0 \equiv & H_{\mathrm{d}} + \sum_\alpha H_\alpha \\ = & \sum_{i=0}^{N-1} \varepsilon \left|d_i\right\rangle \left\langle d_i\right| \\ & - \sum_{0\le i<j\le N-1} v_{ij} \left(\left|d_i\right\rangle \left\langle d_j\right| + \left|d_j\right\rangle \left\langle d_i\right|\right) \\ & + \sum_\alpha \int_{-\pi}^{\pi} \frac{dk}{2\pi} E_k \left|k,\alpha\right\rangle \left\langle k,\alpha\right|, \end{aligned} \tag{A2}$$

$$\begin{aligned} H_1 \equiv & \sum_\alpha H_{\mathrm{d},\alpha} \\ = & -\sum_\alpha t_\alpha \int_{-\pi}^{\pi} \frac{dk}{2\pi} \left(\left|k,\alpha\right\rangle \left\langle d_0\right| + \left|d_0\right\rangle \left\langle k,\alpha\right|\right), \end{aligned} \tag{A3}$$

the state $|k,\alpha\rangle$ is an eigenstate of H_0 (more specifically, of H_α) with the eigenvalue $E_k = -2t\cos k$, and δ is a positive infinitesimal ensuring that the solution is an outgoing wave.

The formal solution of the Lippmann-Schwinger equation (A1) is given in the form

$$\begin{aligned} \left|\psi^{\mathrm{F}}_{k,\alpha}\right\rangle = & |k,\alpha\rangle + \frac{1}{E_k - H + i\delta} H_1 \left|k,\alpha\right\rangle \\ = & |k,\alpha\rangle - \frac{t_\alpha}{E_k - H + i\delta} \left|d_0\right\rangle. \end{aligned} \tag{A4}$$

Using the resolution of unity

$$1 = \sum_{i=0}^{N-1} \left|d_i\right\rangle \left\langle d_i\right| + \sum_\beta \int_{-\pi}^{\pi} \frac{dq}{2\pi} \left|q,\beta\right\rangle \left\langle q,\beta\right|, \tag{A5}$$

we then have

$$\begin{aligned} \left|\psi^{\mathrm{F}}_{k,\alpha}\right\rangle = |k,\alpha\rangle - t_\alpha \Bigg(& \sum_{i=0}^{N-1} G^{\mathrm{R}}_{i0}(E_k) \left|d_i\right\rangle \\ & + \sum_\beta \int_{-\pi}^{\pi} \frac{dq}{2\pi} \left\langle q,\beta\right| \frac{1}{E_k - H + i\delta} \left|d_0\right\rangle \left|q,\beta\right\rangle \Bigg), \end{aligned} \tag{A6}$$

where

$$G^{\mathrm{R}}_{ij}(E_k) \equiv \left\langle d_i\right| \frac{1}{E_k - H + i\delta} \left|d_j\right\rangle. \tag{A7}$$

In order to transform the final term on the right-hand side of Eq. (A6), we calculate the following:

$$\begin{aligned} & \frac{1}{E_k - H - i\delta} \left|q,\beta\right\rangle \\ & = \left(1 + \frac{1}{E_k - H - i\delta} H_1\right) \frac{1}{E_k - H_0 - i\delta} \left|q,\beta\right\rangle \\ & = \frac{1}{E_k - E_q - i\delta} \left(\left|q,\beta\right\rangle - \frac{t_\beta}{E_k - H - i\delta} \left|d_0\right\rangle\right). \end{aligned} \tag{A8}$$

We thereby have

$$\left\langle q,\beta\right| \frac{1}{E_k - H + i\delta} \left|d_0\right\rangle = -t_\beta G^{\mathrm{R}}_{00}(E_k). \tag{A9}$$

We therefore arrive at

$$\begin{aligned} |\psi^{\mathrm{F}}_{k,\alpha}\rangle = & |k,\alpha\rangle - t_\alpha \Bigg(\sum_{i=0}^{N-1} G^{\mathrm{R}}_{i0}(E_k) |d_i\rangle \\ & - G^{\mathrm{R}}_{00}(E_k) \sum_\beta \int_{-\pi}^{\pi} \frac{dq}{2\pi} \frac{t_\beta |q,\beta\rangle}{E_k - E_q + i\delta} \Bigg). \end{aligned} \tag{A10}$$

We describe in Appendix C how we can calculate the Green's function G^{R}_{ij}.

APPENDIX B: PROOF OF EQ. (28)

In the present Appendix, we prove Eq. (28). Using the expression (A10) of the scattering state, we have

$$\begin{aligned} \langle d_i|\psi^{\mathrm{F}}_k\rangle\langle\tilde{\psi}^{\mathrm{F}}_k|d_j\rangle = & \sum_\alpha \langle d_i|\psi^{\mathrm{F}}_{k,\alpha}\rangle\langle\tilde{\psi}^{\mathrm{F}}_{k,\alpha}|d_j\rangle \\ = & \sum_\alpha {t_\alpha}^2 G^{\mathrm{R}}_{i0}(E_k) G^{\mathrm{A}}_{0j}(E_k). \end{aligned} \tag{B1}$$

We therefore have

$$\begin{aligned}
&\int \frac{dk}{2\pi}\frac{\langle d_i|\psi_k^{\mathrm{F}}\rangle\langle\tilde{\psi}_k^{\mathrm{F}}|d_j\rangle}{E-E_k}\\
&=\sum_\alpha {t_\alpha}^2 \int \frac{dk}{2\pi}\frac{1}{E+t\left(e^{ik}+e^{-ik}\right)}\\
&\qquad\times \langle d_i|\frac{1}{E-H_{\mathrm{d}}-\sum_\alpha ({t_\alpha}^2/t)e^{ik}|d_0\rangle\langle d_0|}|d_0\rangle\\
&\qquad\times \langle d_0|\frac{1}{E-H_{\mathrm{d}}-\sum_\alpha ({t_\alpha}^2/t)e^{-ik}|d_0\rangle\langle d_0|}|d_j\rangle, \quad \text{(B2)}
\end{aligned}$$

where we used Eq. (C14) for the Green's functions with the expression (C33) for the effective potential.

On the paths $C_\parallel^{\mathrm{R}}(\kappa_0)$ and $C_\parallel^{\mathrm{A}}(\kappa_0)$, we let $k=k_{\mathrm{r}}\pm i\kappa_0$ and integrate with respect to k_{r}. For $k=k_{\mathrm{r}}+i\kappa_0$, the element e^{-ik} grows in the limit $\kappa_0\to\infty$ in the denominators of two of the three factors on the right-hand side of Eq. (B2). For $k=k_{\mathrm{r}}-i\kappa_0$, the element e^{ik} grows in the limit $\kappa_0\to\infty$ again in the denominators of two of the three factors. Therefore the integral (B2) vanishes on the paths $C_\parallel^{\mathrm{R}}(\kappa_0)$ and $C_\parallel^{\mathrm{A}}(\kappa_0)$ in the limit $\kappa_0\to\infty$. Thus Eq. (28) is proved for the system (12).

APPENDIX C: THE GREEN'S FUNCTION IN THE CENTRAL DOT AND CALCULATION OF THE RESONANCES

In this appendix, we describe the calculation of the Green's function $G_{ij}^{\mathrm{R}}(E)$ for the states in the central dot, $\{|d_i\rangle\}$. The calculation utilizes the self-energy of the semi-infinite leads [2, 85, 86, 99, 100, 101, 102, 103, 104, 105, 106, 107, 108]. Using the expression of the Green's function, we also give an equation that gives the resonant states.

The basic statement is the fact

$$G_{ij}^{\mathrm{R}}(E)\equiv\langle d_i|\,\frac{1}{E-H+i\delta}\,|d_j\rangle=\langle d_i|\,\frac{1}{E-H_{\mathrm{eff}}^{\mathrm{R}}(E)}\,|d_j\rangle\,, \quad \text{(C1)}$$

where the thus-defined effective Hamiltonian $H_{\mathrm{eff}}^{\mathrm{R}}$ has degrees of freedom only on the central dot. Below, we will review the derivation of the following form:

$$H_{\mathrm{eff}}^{\mathrm{R}}(E)=H_{\mathrm{d}}+V_{\mathrm{eff}}^{\mathrm{R}}(E)|d_0\rangle\langle d_0|, \quad \text{(C2)}$$

where

$$\begin{aligned}
H_{\mathrm{d}}\equiv&\sum_{i=0}^{N-1}\varepsilon_i|d_i\rangle\langle d_i|\\
&-\sum_{0\le i<j\le N-1}v_{ij}\left(|d_i\rangle\langle d_j|+|d_j\rangle\langle d_i|\right), \quad \text{(C3)}
\end{aligned}$$

$$V_{\mathrm{eff}}^{\mathrm{R}}(E)\equiv\sum_\alpha\left(\frac{t_\alpha}{t}\right)^2\frac{E-i\sqrt{4t^2-E}}{2}. \quad \text{(C4)}$$

Therefore, we can calculate the Green's function G_{ij}^{R} by inverting an $N\times N$ matrix (C2).

There are several ways of deriving Eq. (C1). One way is to use the resolvent expansion

$$\begin{aligned}
\frac{1}{E-H+i\delta}=&\frac{1}{E-H_0+i\delta}\\
&+\frac{1}{E-H_0+i\delta}H_1\frac{1}{E-H_0+i\delta}\\
&+\frac{1}{E-H_0+i\delta}H_1\frac{1}{E-H_0+i\delta}H_1\frac{1}{E-H_0+i\delta}\quad+\cdots, \quad \text{(C5)}
\end{aligned}$$

where

$$\begin{aligned}
H_0\equiv&H_{\mathrm{d}}+\sum_\alpha H_\alpha\\
=&\sum_{i=0}^{N-1}\varepsilon\,|d_i\rangle\,\langle d_i|\\
&-\sum_{0\le i<j\le N-1}v_{ij}\left(|d_i\rangle\,\langle d_j|+|d_j\rangle\,\langle d_i|\right)\\
&-t\sum_\alpha\sum_{x_\alpha=0}^{\infty}\left(|x_\alpha+1\rangle\langle x_\alpha|+|x_\alpha\rangle\langle x_\alpha+1|\right) \quad \text{(C6)}
\end{aligned}$$

$$\begin{aligned}
H_1\equiv&\sum_\alpha H_{\mathrm{d},\alpha}\\
=&-\sum_\alpha t_\alpha\left(|x_\alpha=0\rangle\,\langle d_0|+|d_0\rangle\,\langle x_\alpha=0|\right) \quad \text{(C7)}
\end{aligned}$$

In calculating $G_{ij}^{\mathrm{R}}(E)$ defined in Eq. (C1), we should note the following. Let $\mathcal{H}_{\mathrm{d}}$ denote the Hilbert space spanned by the states on the central dot, $\{|d_i\rangle\}$, and $\mathcal{H}_{\mathrm{lead}}$ denote the Hilbert space spanned by the states on the leads, $\{|x_\alpha\rangle\}$. Then we have

$$\frac{1}{E-H_0+i\delta}|d_i\rangle=\frac{1}{E-H_{\mathrm{d}}+i\delta}|d_i\rangle\in\mathcal{H}_{\mathrm{d}}, \quad \text{(C8)}$$

$$\frac{1}{E-H_0+i\delta}|x_\alpha\rangle=\frac{1}{E-H_\alpha+i\delta}|x_\alpha\rangle\in\mathcal{H}_{\mathrm{lead}}, \quad \text{(C9)}$$

$$H_1|d_i\rangle=-\delta_{0i}\sum_\alpha t_\alpha|x_\alpha=0\rangle\in\mathcal{H}_{\mathrm{lead}}, \quad \text{(C10)}$$

$$H_1|x_\alpha\rangle=-\delta_{x_\alpha 0}t_\alpha|d_0\rangle\in\mathcal{H}_{\mathrm{d}}. \quad \text{(C11)}$$

That is, the operator $(E-H_0+i\delta)^{-1}$, when applied to a state either in $\mathcal{H}_{\mathrm{d}}$ or $\mathcal{H}_{\mathrm{lead}}$, does not change its Hilbert space, whereas the operator H_1 switches it. Therefore, all terms of odd orders of H_1 in the resolvent expansion of G_{ij}^{R} vanish. All terms of even orders of H_1 (except the zeroth order) have powers of the following factor:

$$\begin{aligned}
&\sum_\alpha\langle d_0|H_1|x_\alpha=0\rangle\\
&\qquad\times\langle x_\alpha=0|\frac{1}{E-H_0+i\delta}|x_\alpha=0\rangle\\
&\qquad\times\langle x_\alpha=0|H_1|d_0\rangle\\
&=\sum_\alpha {t_\alpha}^2\langle x_\alpha=0|\frac{1}{E-H_\alpha+i\delta}|x_\alpha=0\rangle. \quad \text{(C12)}
\end{aligned}$$

We will show below that this quantity is equal to $V^{\mathrm{R}}_{\mathrm{eff}}(E)$ defined in Eq. (C4). We therefore have

$$\begin{aligned} & G^{\mathrm{R}}_{ij}(E) \\ & = \langle d_i | \frac{1}{E - H_{\mathrm{d}} + i\delta} | d_j \rangle \\ & \quad + \langle d_i | \frac{1}{E - H_{\mathrm{d}} + i\delta} | d_0 \rangle V^{\mathrm{R}}_{\mathrm{eff}} \langle d_0 | \frac{1}{E - H_{\mathrm{d}} + i\delta} | d_j \rangle \\ & \quad \cdots , \end{aligned} \tag{C13}$$

which can be summarized as

$$G^{\mathrm{R}}_{ij}(E) = \langle d_i | \frac{1}{E - H_{\mathrm{d}} - |d_0\rangle V^{\mathrm{R}}_{\mathrm{eff}} \langle d_0| + i\delta} | d_j \rangle. \tag{C14}$$

The remaining task is to calculate $\langle x_\alpha = 0 | (E - H_0 + i\delta)^{-1} | x_\alpha = 0 \rangle$ in Eq. (C12), or

$$G^{\mathrm{R}}_{\mathrm{lead}}(E; 0) \equiv \langle x = 0 | \frac{1}{E - H_{\mathrm{lead}}(0) + i\delta} | x = 0 \rangle, \tag{C15}$$

where

$$H_{\mathrm{lead}}(X) = -t \sum_{x=X}^{\infty} \left(|x+1\rangle\langle x| + |x\rangle\langle x+1| \right). \tag{C16}$$

We then use the resolvent expansion

$$\begin{aligned} & \frac{1}{E - H_{\mathrm{lead}}(0) + i\delta} = \frac{1}{E - H_{\mathrm{lead}}(1) + i\delta} \\ & + \frac{1}{E - H_{\mathrm{lead}}(1) + i\delta} \\ & \quad \times (-t) \left(|1\rangle\langle 0| + |0\rangle\langle 1| \right) \frac{1}{E - H_{\mathrm{lead}}(1) + i\delta} \\ & + \cdots . \end{aligned} \tag{C17}$$

Similar reasoning as the one described in Eqs. (C5)–(C14) leads us to

$$G^{\mathrm{R}}_{\mathrm{lead}}(E; 0) = \frac{1}{E - t^2 G^{\mathrm{R}}_{\mathrm{lead}}(E; 1) + i\delta} \tag{C18}$$

with

$$G^{\mathrm{R}}_{\mathrm{lead}}(E; 1) = \langle x = 1 | \frac{1}{E - H_{\mathrm{lead}}(1) + i\delta} | x = 1 \rangle. \tag{C19}$$

Thanks to the translational invariance, we should have $G^{\mathrm{R}}_{\mathrm{lead}}(E; 0) = G^{\mathrm{R}}_{\mathrm{lead}}(E; 1)$. Then, Eq. (C18) reduces to a quadratic equation

$$t^2 \left(G^{\mathrm{R}}_{\mathrm{lead}} \right)^2 - E G^{\mathrm{R}}_{\mathrm{lead}} + 1 = 0, \tag{C20}$$

which is followed by

$$G^{\mathrm{R}}_{\mathrm{lead}}(E; 0) = \frac{E - i\sqrt{4t^2 - E^2}}{2t^2} \qquad \text{for } -2t \le E \le 2t, \tag{C21}$$

where we fixed the sign in front of the square root so that the imaginary part may be negative. Thus the quantity (C12) was indeed shown to be equal to $V^{\mathrm{R}}_{\mathrm{eff}}(E)$ defined in Eq. (C4).

To summarize the above, the retarded Green's function given by (C14) is expressed in the form (C1) with the effective potential $V^{\mathrm{R}}_{\mathrm{eff}}$ defined in Eq. (C4). The Green's functions that are used in the expression of the scattering state (A10) are therefore obtained by inverting the $N \times N$ matrix $\langle d_i | (E - H^{\mathrm{R}}_{\mathrm{eff}}(E)) | d_j \rangle$ for a fixed value of E. Incidentally, the infinitesimal $+i\delta$ in the denominator of the definition (C1) is not necessary anymore because $V^{\mathrm{R}}_{\mathrm{eff}}$ already has an imaginary part. In fact, the advanced Green's function is given by flipping the sign of the imaginary part;

$$G^{\mathrm{A}}_{ij}(E) \equiv \langle d_i | \frac{1}{E - H - i\delta} | d_j \rangle = \langle d_i | \frac{1}{E - H^{\mathrm{A}}_{\mathrm{eff}}(E)} | d_j \rangle \tag{C22}$$

with

$$V^{\mathrm{A}}_{\mathrm{eff}}(E) \equiv \sum_{\alpha} \left(\frac{t_\alpha}{t} \right)^2 \frac{E + i\sqrt{4t^2 - E}}{2}. \tag{C23}$$

Although we have derived the expression (C1) particularly for the present system (12) with all the leads attached to a single site, the expression (C1) itself holds for more general systems with appropriate changes of definition of the effective Hamiltonian (C2); see Refs. [2, 85, 86, 99]. We can reduce the calculation of the Green's function further for the present system (12), using the resolvent expansion (C13) again. For $i = j = 0$, Eq. (C13) now gives

$$\begin{aligned} G^{\mathrm{R}}_{00}(E) = & G^{\mathrm{d}}_{00}(E) \\ & + G^{\mathrm{d}}_{00}(E) V^{\mathrm{R}}_{\mathrm{eff}}(E) G^{\mathrm{d}}_{00}(E) \\ & + G^{\mathrm{d}}_{00}(E) V^{\mathrm{R}}_{\mathrm{eff}}(E) G^{\mathrm{d}}_{00}(E) V^{\mathrm{R}}_{\mathrm{eff}}(E) G^{\mathrm{d}}_{00}(E) \\ & + \cdots , \end{aligned} \tag{C24}$$

where

$$G^{\mathrm{d}}_{00}(E) \equiv \langle d_0 | \frac{1}{E - H_{\mathrm{d}}} | d_0 \rangle. \tag{C25}$$

Summing the series we obtain

$$G^{\mathrm{R}}_{00}(E) = \frac{1}{(G^{\mathrm{d}}_{00}(E))^{-1} - V^{\mathrm{R}}_{\mathrm{eff}}(E)} \tag{C26}$$

This reduces the calculation of G^{R}_{00} from inversion of an non-Hermitian matrix $(E - H^{\mathrm{R}}_{\mathrm{eff}})$ to a Hermitian matrix $(E - H_{\mathrm{d}})$. For $j = 0$ or $i = 0$, we have

$$G^{\mathrm{R}}_{i0} = \frac{G^{\mathrm{d}}_{i0}}{1 - G^{\mathrm{d}}_{00} V^{\mathrm{R}}_{\mathrm{eff}}}, \tag{C27}$$

$$G^{\mathrm{R}}_{0j} = \frac{G^{\mathrm{d}}_{0j}}{1 - G^{\mathrm{d}}_{00} V^{\mathrm{R}}_{\mathrm{eff}}}, \tag{C28}$$

respectively, and for general i and j we have

$$G^{\mathrm{R}}_{ij} = G^{\mathrm{d}}_{ij} + G^{\mathrm{d}}_{i0}\frac{V^{\mathrm{R}}_{\mathrm{eff}}}{1 - G^{\mathrm{d}}_{00}V^{\mathrm{R}}_{\mathrm{eff}}}G^{\mathrm{d}}_{0j}. \tag{C29}$$

Now we show how we can calculate all resonant states for the system (12). As is evident in the Fisher-Lee relation (41), the conductance of the present system has poles in the complex energy plane wherever the Green's function $G^{\mathrm{R}}_{00}(E)$ has poles. The expression (C26) immediately gives the equation for the resonant states in the form

$$G^{\mathrm{d}}_{00}(E)V^{\mathrm{R}}_{\mathrm{eff}}(E) = 1. \tag{C30}$$

The resonant states given for the examples in Sec. IV were thus calculated. Equation (C30) holds particularly for the present system (12) with all the leads attached to a single site. For more general case, the Green's function G^{R}_{00} is given by inversion of the matrix $(E - H^{\mathrm{R}}_{\mathrm{eff}}(E))$. Therefore, all resonant states can be calculated by solving the equation

$$\det(E - H^{\mathrm{R}}_{\mathrm{eff}}(E)) = 0. \tag{C31}$$

The above discussion leads us to a much simpler way of deriving Eq. (C1) [99]; we formulate the Green's function so that it may have poles for the resonant states. Since a resonant state satisfies the boundary condition (6), we have

$$\langle x_\alpha + 1|\psi^{\mathrm{res}}\rangle = e^{ik^{\mathrm{res}}}\langle x_\alpha|\psi^{\mathrm{res}}\rangle \tag{C32}$$

with $\operatorname{Re} k^{\mathrm{res}} \geq 0$. This terminates the Schrödinger equation for the semi-infinite leads with the effective potential

$$V^{\mathrm{R}}_{\mathrm{eff}}(E_k) = -\sum_{\alpha}\frac{{t_\alpha}^2}{t}e^{ik}. \tag{C33}$$

Solving the dispersion relation $E_k = -2t\cos k = -t(e^{ik} + e^{-ik})$, we have

$$e^{ik} = \frac{-E_k + i\sqrt{4t^2 - {E_k}^2}}{2t}, \tag{C34}$$

which again gives Eq. (C4). See Ref. [99] for details.

APPENDIX D: CHOOSING THE SIGN OF THE SOLUTION TO THE RICCATI EQUATION

In this appendix we will derive a criterion to choose either the plus or the minus sign in the solution to the matrix Riccati equation, Eqs. (38) and (39). We will consider the matrix element $G^{\mathrm{R}}_{00}(E) \equiv \langle d_0|G^{\mathrm{R}}(E)|d_0\rangle$, which appears in the conductance (41). For $i = j = 0$, the equation (36) reduces to

$$iG^{\mathrm{R}}_{00}\Gamma_{00}G^{\mathrm{R}}_{00} + G^{\mathrm{R}}_{00}(2 + i\Gamma_{00}\Lambda_{00}) + \Lambda_{00} = 0, \tag{D1}$$

where $G^{\mathrm{R}}_{00} \equiv \langle d_0|G^{\mathrm{R}}(E)|d_0\rangle$, $\Lambda_{00} \equiv \langle d_0|\Lambda(E)|d_0\rangle$, $\Gamma_{00} \equiv \langle d_0|\Gamma(E)|d_0\rangle$ and we made use of the fact that the matrix Γ has only the $(0,0)$ element, Γ_{00}, for the present system (12); see Eq. (32). The solution is given by

$$G^{\mathrm{R}}_{00} = \frac{\Lambda_{00}}{2} + \frac{1}{i\Gamma_{00}}\left[1 \pm \sqrt{1 - \left(\frac{\Gamma_{00}\Lambda_{00}}{2}\right)^2}\right]. \tag{D2}$$

We here use Eqs. (29) and (31) for $i = j = 0$, which gives

$$\Lambda_{00} = G^{\mathrm{A}}_{00} + G^{\mathrm{R}}_{00}, \tag{D3}$$

$$i\Gamma_{00} = \frac{G^{\mathrm{A}}_{00} - G^{\mathrm{R}}_{00}}{G^{\mathrm{A}}_{00}G^{\mathrm{R}}_{00}}. \tag{D4}$$

The solution (D2) then may be written as

$$G^{\mathrm{R}}_{00} = \frac{G^{\mathrm{A}}_{00} + G^{\mathrm{R}}_{00}}{2} + \frac{2G^{\mathrm{A}}_{00}G^{\mathrm{R}}_{00} \pm \sqrt{\left[\left(G^{\mathrm{A}}_{00}\right)^2 + \left(G^{\mathrm{R}}_{00}\right)^2\right]^2}}{2\left(G^{\mathrm{A}}_{00} - G^{\mathrm{R}}_{00}\right)} \tag{D5}$$

This gives a consistent solution to Eq. (D2) if we choose the ± sign as follows:

$$\text{Choose “+” if } \left(G^{\mathrm{A}}_{00}\right)^2 + \left(G^{\mathrm{R}}_{00}\right)^2 < 0; \tag{D6}$$

$$\text{Choose “−” if } \left(G^{\mathrm{A}}_{00}\right)^2 + \left(G^{\mathrm{R}}_{00}\right)^2 > 0. \tag{D7}$$

Since $G^{\mathrm{R}}_{00} = \left(G^{\mathrm{A}}_{00}\right)^*$ for real E, we have

$$\left(G^{\mathrm{A}}_{00}\right)^2 + \left(G^{\mathrm{R}}_{00}\right)^2 = 2\left(\operatorname{Re} G^{\mathrm{R}}_{00}\right)^2 - 2\left(\operatorname{Im} G^{\mathrm{R}}_{00}\right)^2, \tag{D8}$$

and hence we can write Eq. (D6) as follows:

$$\text{Choose “+” if } \left|\operatorname{Re} G^{\mathrm{R}}_{00}\right| < \left|\operatorname{Im} G^{\mathrm{R}}_{00}\right|; \tag{D9}$$

$$\text{Choose “−” if } \left|\operatorname{Re} G^{\mathrm{R}}_{00}\right| > \left|\operatorname{Im} G^{\mathrm{R}}_{00}\right|. \tag{D10}$$

By using the expression (C26) of the Green's function, we can further reduce the above criterion as follows:

$$\text{Choose “+” if } \left|\left(G^{\mathrm{d}}_{00}\right)^{-1} - \frac{E}{2}\sum_{\alpha}\left(\frac{t_\alpha}{t}\right)^2\right| < \frac{\Gamma_{00}}{2}; \tag{D11}$$

$$\text{Choose “−” if } \left|\left(G^{\mathrm{d}}_{00}\right)^{-1} - \frac{E}{2}\sum_{\alpha}\left(\frac{t_\alpha}{t}\right)^2\right| > \frac{\Gamma_{00}}{2}. \tag{D12}$$

This is the criterion to choose the sign in Eq. (D2). Using Eqs. (C27)–(C29), we can show that this same criterion applies to Eqs. (36) and (37).

---

[1] E. Tekman and P. F. Bagwell, Phys. Rev. B **48**, 2553 (1993).
[2] S. Datta, *Electronic Transport in Mesoscopic Systems* (Cambridge University Press, Cambridge, 1995).
[3] E. R. Racec and U. Wulf, Phys. Rev. B **64**, 115318 (2001).
[4] A. A. Clerk, X. Waintal, and P. W. Brouwer, Phys. Rev. Lett. **86**, 4636 (2001).
[5] H. Lu, R. Lü, and B. F. Zhu, Phys. Rev. B **71**, 235320 (2005).
[6] A. Chakrabarti, Phys. Rev. B **74**, 205315 (2006).
[7] Y. S. Joe, E. R. Hedin, and A. M. Satanin, Phys. Rev. B **76**, 085419 (2007).
[8] S. Fujimoto and Y. Natsume, J. Phys. Soc. Jpn. **77**, 024712 (2008).
[9] K. Kobayashi, H. Aikawa, S. Katsumoto, and Y. Iye, Phys. Rev. Lett. **88**, 256806 (2002).
[10] K. Kobayashi, H. Aikawa, S. Katsumoto, and Y. Iye, Phys. Rev. B **68**, 235304 (2003).
[11] K. Kobayashi, H. Aikawa, A. Sano, S. Katsumoto, and Y. Iye, Phys. Rev. B **70**, 035319 (2004).
[12] M. Sato, H. Aikawa, K. Kobayashi, S. Katsumoto, and Y. Iye, Phys. Rev. Lett. **95**, 066801 (2005).
[13] I. G. Zacharia, D. Goldhaber-Gordon, G. Granger, M. A. Kastner, and Y. B. Khavin, Phys. Rev. B **64**, 155311 (2001).
[14] J. Kim, J. R. Kim, J. O. Lee, J. W. Park, H. M. So, N. Kim, K. Kang, K. H. Yoo, and J. J. Kim, Phys. Rev. Lett. **90**, 166403 (2003).
[15] B. Babić and C. Schönenberger, Phys. Rev. B **70**, 195408 (2004).
[16] D. Brisker, I. Cherkes, C. Gnodtke, D. Jarukanont, S. Klaiman, W. Koch, S. Weissman, R. Volkovich, M. C. Toroker, and U. Peskin, Mol. Phys. **106**, 281 (2008).
[17] K. Sasada and N. Hatano, Physica E **29**, 609 (2005).
[18] N. Hatano, K. Sasada, H. Nakamura, and T. Petrosky, Prog. Theor. Phys. **119**, 187 (2007).
[19] J. Göres, D. Goldhaber-Gordon, S. Heemeyer, M. A. Kastner, H. Shtrikman, D. Mahalu, and U. Meirav, Phys. Rev. B **62**, 2188 (2000).
[20] G. Gamow, Z. Phys. A **51**, 204 (1928).
[21] A. J. F. Siegert, Phys. Rev. **56**, 750 (1939).
[22] R. E. Peierls, Proc. Roy. Soc. London A **253**, 16 (1959).
[23] K. J. le Couteur, Proc. Roy. Soc. London A **256**, 115 (1960).
[24] Y. B. Zel'dovich, J. Expetl. Theoret. Phys. (U.S.S.R.) **39**, 776 (1960), [Sov. Phys. JETP **12**, 542 (1961)].
[25] N. Hokkyo, Prog. Theor. Phys. **33**, 1116 (1965).
[26] W. J. Romo, Nucl. Phys. A **116**, 618 (1968).
[27] T. Berggren, Phys. Lett. **33B**, 547 (1970).
[28] B. Gyarmati and T. Vertse, Nucl. Phys. A **160**, 523 (1971).
[29] W. J. Romo, J. Math. Phys. **21**, 311 (1980).
[30] T. Berggren, Nucl. Phys. A **389**, 261 (1982).
[31] T. Berggren, Phys. Lett. B **373**, 1 (1996).
[32] R. de la Madrid, G. García-Calderón, and J. Muga, Czech. J. Phys. **55**, 1141 (2005).
[33] C. Eckart, Phys. Rev. **35**, 1303 (1930).
[34] H. A. Bethe and R. F. Bacher, Rev. Mod. Phys. **8**, 82 (1936).
[35] L. Hulthén, Arkiv Matematik Astronomi Fysik **28A, No. 5**, 1 (1942).
[36] L. Hulthén, Arkiv Mat. Astr. Fysik **29B, No. 1**, 1 (1942).
[37] R. Jost and A. Pais, Phys. Rev. **82**, 840 (1951).
[38] E. Vogt and G. H. Wannier, Phys. Rev. **95**, 1190 (1954).
[39] E. P. Wigner, Phys. Rev. **98**, 145 (1955).
[40] E. Corinaldesi, Nucl. Phys. **2**, 420 (1956).
[41] H. M. Nussenzveig, Nucl. Phys. **11**, 499 (1959).
[42] D. I. Fivel and A. Klein, J. Math. Phys. **1**, 274 (1960).
[43] J. Humblet and L. Rosenfeld, Nucl. Phys. **26**, 529 (1961).
[44] L. Rosenfeld, Nucl. Phys. **26**, 594 (1961).
[45] J. Humblet, Nucl. Phys. **31**, 544 (1962).
[46] J. Humblet, Nucl. Phys. **50**, 1 (1964).
[47] J. P. Jeukenne, Nucl. Phys. **58**, 1 (1964).
[48] J. Humblet, Nucl. Phys. **57**, 386 (1964).
[49] C. Mahaux, Nucl. Phys. **68**, 471 (1965).
[50] L. Rosenfeld, Nucl. Phys. **70**, 1 (1965).
[51] A. Bhattacharjie and E. C. G. Sudarshan, Il Nuovo Cimento **25**, 864 (1962).
[52] L. Wojtczak, Nucl. Phys. **48**, 325 (1963).
[53] R. M. Spector, J. Math. Phys. **5**, 1185 (1964).
[54] A. K. Bose, Il Nuovo Cimento **32**, 679 (1964).
[55] H. H. Aly and R. M. Spector, Il Nuovo Cimento **38**, 149 (1965).
[56] K. W. McVoy, L. Heller, and M. Bolsterli, Rev. Mod. Phys. **39**, 245 (1967).
[57] O. P. Bahethi and M. G. Fuda, J. Math. Phys. **12**, 2076 (1971).
[58] M. G. Fuda, J. Math. Phys. **12**, 1163 (1971).
[59] M. Bawin and J. P. Lavine, Il Nuovo Cimento **23A**, 311 (1974).
[60] G. D. Doolen, Int. J. Quant. Chem. **14**, 523 (1978).
[61] H. Narnhofer and W. Thirring, Phys. Rev. A **23**, 1688 (1981).
[62] M. Rittby, N. Elander, and E. Brändas, Mol. Phys. **45**, 553 (1982).
[63] Y. Alhassid, F. Iachello, and R. D. Levine, Phys. Rev. Lett. **54**, 1746 (1985).
[64] H. Massmann, Am. J. Phys. **53**, 679 (1985).
[65] D. T. Colbert, R. Mayrhofer, and P. R. Certain, Phys. Rev. A **33**, 3560 (1986).
[66] I. Benjamin and R. D. Levine, Phys. Rev. A **33**, 2833 (1986).
[67] W. O. Amrein and M. B. Cibils, Helv. Phys. Acta **60**, 481 (1987).
[68] A. Bohm, M. Gadella, and G. B. Mainland, Am. J. Phys. **57**, 1103 (1989).
[69] J. N. Ginocchio, Ann. Phys. **152**, 203 (1984).
[70] S. A. Rakityansky, S. A. Sofianos, and K. Amos, Il Nuovo Cimento **111B**, 363 (1996).
[71] M. Homma, T. Myo, and K. Katō, Prog. Theor. Phys. **97**, 561 (1997).
[72] H. Masui, S. Aoyama, T. Myo, and K. Katō, Prog. Theor. Phys. **102**, 1119 (1999).
[73] H. Barkay and N. Moiseyev, Phys. Rev. A **64**, 044702 (2001).
[74] C. A. A. de Carvalho and H. Nussenzveig, Phys. Rep. **364**, 83 (2002).
[75] M. Razavy, *Quantum Theory of Tunneling* (World Scientific, Singapore, 2003).

[76] Z. Ahmed and S. R. Jain, J. Phys. A: Math. Gen. **37**, 867 (2004).

[77] N. G. Kelkar, M. Nowakowski, K. P. Khemchandani, and S. R. Jain, Nucl. Phys. A **730**, 121 (2004).

[78] S. R. Jain, Phys. Lett. A **335**, 83 (2005).

[79] W. O. Amrein and K. B. Sinha, J. Phys. A: Math. Gen. **39**, 9231 (2006).

[80] N. Moiseyev, M. Šindelka, and L. S. Cederbaum, J. Phys. B: At. Mol. Opt. Phys. **41**, 221001 (2008).

[81] I. Rotter, J. Phys. A: Math. Theor. **42**, 153001 (2009).

[82] U. Fano, Phys. Rev. **124**, 1866 (1961).

[83] T. N. Rescigno, M. Baertschy, D. Byrum, and C. W. McCurdy, Phys. Rev. A **55**, 4253 (1997).

[84] L. D. Landau and E. M. Lifshitz, *Quantum Mechanics (Non-relativistic Theory), 3rd edition* (Pergamon Press, Oxford, 1977).

[85] H. Kunz and B. Shapiro, J. Phys. A: Math. Gen. **39**, 10155 (2006).

[86] H. Kunz and B. Shapiro, Phys. Rev. B **77**, 054203 (2008).

[87] N. Nakanishi, Prog. Theor. Phys. **19**, 607 (1958).

[88] T. Petrosky, I. Prigogine, and S. Tasaki, Physica A **173**, 175 (1991).

[89] H. O. Ohanian and C. G. Ginsburg, Am. J. Phys. **42**, 310 (1974).

[90] K. O. Friedrichs, Commun. Pure Appl. Math. **1**, 361 (1948).

[91] P. W. Anderson, Phys. Rev. **124**, 41 (1961).

[92] E. C. G. Sudershan, *Structure of Dynamical Theories* (W. A. Benjamin, New York, 1962).

[93] G. Ordonez, T. Petrosky, and I. Prigogine, Phys. Rev. A **63**, 052106 (2001).

[94] M. Miyamoto, Phys. Rev. A **70**, 032108 (2004).

[95] M. Miyamoto, Phys. Rev. A **72**, 063405 (2005).

[96] R. G. Newton, *Scattering Theory of Waves and Particles, 2nd edition* (Springer-Verlag, New York, 1982).

[97] D. S. Fisher and P. A. Lee, Phys. Rev. B **23**, 6851 (1981).

[98] I. Maruyama, N. Shibata, and K. Ueda, J. Phys. Soc. Jpn. **73**, 3239 (2004).

[99] K. Sasada and N. Hatano, J. Phys. Soc. Jpn. **77**, 025003 (2008).

[100] M. S. Livshits, J. Exptl. Theoret. Phys. (U.S.S.R.) **31**, 121 (1956), [Sov. Phys. JETP, 4, 91-98 (1957)].

[101] H. Feshbach, Ann. Phys. (New York) **5**, 357 (1958).

[102] H. Feshbach, Ann. Phys. (New York) **19**, 287 (1962).

[103] S. Albeverio, F. Haake, P. Kurasov, M. Kuś, and P. Šeba, J. Math. Phys. **37**, 4888 (1996).

[104] Y. V. Fyodorov and H.-J. Sommers, J. Math. Phys. **38**, 1918 (1997).

[105] F.-M. Dittes, Phys. Rep. **339**, 215 (2000).

[106] H. S. K. Pichugin and P. Šeba, Phys. Rev. E **64**, 056227 (2001).

[107] A. F. Sadreev and I. Rotter, J. Phys. A: Math. Gen. **36**, 11413 (2003).

[108] J. Okołowicz, M. Płoszajczak, and I. Rotter, Phys. Rep. **374**, 271 (2003).